

Composition of the Earth's Lower Mantle

Motohiko Murakami¹, Amir Khan¹, Paolo Sossi¹, Maxim D. Ballmer², and Pinku Saha¹

¹Department of Earth Sciences, ETH Zurich, Zürich, Switzerland, 8092; email: motohiko.murakami@erdw.ethz.ch

²Department of Earth Sciences, University College London, London, UK

Xxxx. Xxx. Xxx. Xxx. YYYY. AA:1–34

[https://doi.org/10.1146/\(\(please add article doi\)\)](https://doi.org/10.1146/((please add article doi)))

Copyright © YYYY by the author(s).
All rights reserved

Keywords

Lower mantle, chemical composition, Mg/Si ratio, mineralogy, seismic structure, density, thermal state, mantle convection, dynamical evolution.

Abstract

Determining the composition of Earth's lower mantle, which constitutes almost half of its total volume, has been a central goal in the Earth sciences for more than a century given the constraints it places on Earth's origin and evolution. However, whether the major-element chemistry of the lower mantle, in the form of, e.g., Mg/Si ratio is similar to or different from the upper mantle remains debated. Here, we use a multi-disciplinary approach to address the question of the composition of Earth's lower mantle, and, in turn, that of bulk silicate Earth (crust and mantle) by considering the evidence provided by geochemistry, geophysics, mineral physics, and geodynamics. Geochemical and geodynamical evidence largely agrees, indicating a lower-mantle molar Mg/Si of ≥ 1.12 (≥ 1.15 for bulk silicate Earth), consistent with the rock record and accumulating evidence for whole-mantle stirring. However, mineral-physics-informed profiles of seismic properties, based on a lower mantle made of bridgmanite and ferropericlase, points to Mg/Si ~ 0.9 – 1.0 when compared with radial seismic reference models. This highlights the importance of considering the presence of additional minerals (e.g., calcium-perovskite and stishovite) and possibly suggests a lower mantle varying compositionally with depth. In closing, we discuss how we can improve our understanding of lower-mantle and bulk silicate Earth composition, including its impact on the light-element budget of the core.

Contents

1. INTRODUCTION	2
2. Geo- and cosmochemical constraints on Earth's lower mantle composition	4
2.1. Composition of the upper mantle.....	4
2.2. Chemical and isotopic fractionation during Earth's accretion	5
2.3. Evidence for Si in the core	6
2.4. Geochemical constraints on differences in composition between the upper and lower mantle	7
3. Lower mantle composition and thermal state: a geophysical perspective	10
3.1. Mineralogical predictions.....	10
3.2. Methods for geophysical inversion of lower mantle composition	12
4. Experimental mineral physics: constraints from elasticity	13
4.1. Experimental considerations	13
4.2. Constructing lower mantle seismic profiles from experimental data	15
4.3. Combining mineral physics and geophysical constraints	17
5. The composition of Earth's lower mantle in the context of Earth evolution and dynamics	19
5.1. Heterogeneity Formation in the Early Earth.....	19
5.2. Heterogeneity Preservation during Long-term Mantle Evolution	20
5.3. Enrichment of basaltic rocks in the convecting lower mantle	23
5.4. Implications for BSE composition	23
6. Summary	24

1. INTRODUCTION

Earth's mantle is a mineralogical assemblage composed of silicates, principally containing MgO and SiO₂, that make up 80–85% of the mass of the bulk silicate Earth (BSE = mantle and crust) (McDonough and Sun 1995, Palme and O'Neill 2014). It follows that the ratio of these oxides, expressed here as the molar Mg/Si ratio, controls the mineralogy of the mantle. In the upper mantle, high Mg/Si stabilises olivine (Mg,Fe)₂SiO₄ at the expense of orthopyroxene (Mg,Fe)SiO₃, while ferropericlase (Mg,Fe)O replaces bridgmanite (Mg,Fe)SiO₃ in the lower mantle. Owing to its solid solution with Mg in silicate minerals, the quantity of iron, and indeed its valence state (occurring as Fe⁰, Fe²⁺ and Fe³⁺), influences the stability of mantle phases. Therefore, despite its role in establishing mantle mineralogy, and, in turn, physical properties (e.g., density, seismic velocities, viscosity), the composition of the BSE remains poorly constrained, particularly in the lower mantle.

This lack of information stems from the absence of direct samples, meaning geophysical techniques are an important constraint on lower-mantle structure and composition (e.g., Khan 2016). While seismology, because of its higher resolving power relative to other geophysical methods, has provided the most detailed information, electromagnetic sounding, gravity, and geodetic measurements yield complementary information related to the physicochemical state of the mantle (e.g., Koyama et al. 2014, Lau et al. 2016, 2017). Moreover, direct measurements or first-principles simulations of the physical properties of relevant minerals and synthetic analogues at the conditions of the deep Earth allow for comparison with geophysical models that are constrained by field measurements (e.g., da Silva et al. 2000, Murakami et al. 2012). These sources constitute a large complement of information that aid in delineating possible compositions, thermal states and hence mineralogies of Earth's lower mantle (Bina and Helffrich 2014).

Intimately related to the question of Earth's lower mantle composition is that of the building blocks from which the Earth accreted. Chondrites are thought to approximate the bulk composition of the Earth, on the basis of the similarity of the proportions of their major constituents, Mg, Fe, Si, Ca and Al, to those in the Earth's accessible mantle (Ringwood 1966). Yet, this chondritic paradigm is strictly valid only for refractory elements, such as Ca and Al, whose relative abundances among chondrite groups are constant to within $\sim 5\%$, whereas those of more volatile elements, such as Fe, Si and Mg, vary markedly (Wasson and Kallemeyn 1988). Indeed, models for the composition of the BSE based on peridotites, rocks representative of the upper mantle, are found to have higher Mg/Si than among the chondritic meteorites (e.g., Hart and Zindler 1986, Workman and Hart 2005, McDonough and Sun 1995, Lyubetskaya and Korenaga 2007, Palme and O'Neill 2014). This difference could be the result of the accretion of Earth from non-chondritic components (e.g., O'Neill and Palme 2008), the accumulation of Si relative to Mg in the lower mantle and/or the incorporation of Si into the core (Poirier 1994, Allègre et al. 1995). Determining the composition of the lower mantle thus helps to bracket the light-element budget of the core, providing further constraints on accretion, differentiation, and early evolution of our planet.

Should the lower mantle have a chemical composition distinct to that in the upper mantle, then dynamical mechanism(s) must have conspired over Earth's history to engender stratification. Homogeneity in mantle composition on a global scale is often invoked, given that Earth's average upper mantle composition (Ringwood 1975, Workman and Hart 2005), is able to satisfy a large range of geochemical and geophysical observations, including the mean radial mantle seismic velocity structure (e.g., Weidner 1985, Jackson and Rigden 1998), the average depth of the major mantle seismic discontinuities (e.g. Irifune 1994), and the mantle electrical conductivity structure (e.g., Xu et al. 2000, Grayver et al. 2017). Yet, despite these indications of a well-mixed mantle, there is ample seismic evidence to show that the mantle structure is more complex in detail, reflecting changes in temperature, chemical composition (Khan et al. 2009, Cammarano et al. 2005, Schuberth et al. 2009) and lithology, approximated as either mechanical mixtures of basaltic and harzburgitic rocks or an equilibrium assemblages with different bulk compositions (Munch et al. 2020, Waszek et al. 2021, Bissig et al. 2022a,b, Tauzin et al. 2022). Moreover, geodynamical simulations indicate that Earth's mantle may operate in a hybrid regime between layered- and whole-mantle convection, e.g., with intermittent penetration of slabs into the lower mantle (e.g., Tackley et al. 2005). Indeed, lateral variations in rock viscosity and density associated with heterogeneity in Mg/Si (e.g., Xu et al. 2008, 2017, Tsujino et al. 2022) can delay mantle mixing and lead to segregation of distinct material (Manga 1996, Nakagawa and Buffett 2005, Ballmer et al. 2017a, Yan et al. 2020).

In this study, we examine existing geochemical and geophysical data to assess the degree to which the chemical composition of the lower mantle differs, if at all, from that of the upper mantle. To properly frame the problem, the compositions of samples from the upper mantle are compared with a chondritic BSE (section 2). Deviations from the expected chondritic baseline may be accommodated, in part, by chemical differences between the upper- and lower mantle. To determine whether this is the case, and in the absence of lower mantle samples, we turn to geophysics and seismology to provide a new model of the velocity- and density structure of the (lower) mantle (section 3). We contrast these observations with measurements of the physical properties of thermodynamically stable mineral assemblages to constrain the composition and thermal state of the lower mantle (section 4). Then

geodynamic mechanisms are explored that can lead to chemical variability in the convecting mantle over time, within the bounds permitted by geochemical and geophysical observations (section 5). Although these complementary approaches do not converge to a unique lower mantle composition, they attest to abundances of the major elements in the upper and lower mantle lying within $\sim 10\%$ of each other, and preclude drastic mineralogical changes at the whole-mantle scale.

2. Geo- and cosmochemical constraints on Earth's lower mantle composition

2.1. Composition of the upper mantle

Modern models for the composition of the bulk silicate Earth (BSE) exploit the chemical variability in global mantle peridotites to extrapolate to an assumed chondritic Ca/Al ratio (e.g., McDonough and Sun 1995, Palme and O'Neill 2014). This assumption is based on the fact that Ca and Al are both lithophile (i.e., near-absent in the Earth's core) and cosmochemically refractory (i.e., condensing at temperatures higher than those of the major components, Mg, Si and Fe - ~ 1350 K - from a solar composition gas at 10^{-4} bar; Lodders 2003). The Ca/Al ratio of chondrites varies by $\sim 2.5\%$ relative (excluding EL; Wasson and Kallemeyn 1988), such that chondritic ratios among refractory lithophile elements (RLEs) are expected to hold for the Earth. By corollary, there is no requirement for the ratios of the major elements, Fe, Mg and Si, to be chondritic in the Earth. Indeed, the Fe/Mg ratio among chondrites varies by $\sim 40\%$ relative (Wasson and Kallemeyn 1988), rendering the concept of a chondritic composition for these elements a misnomer. Consequently, the composition of the BSE, particularly for Fe, Mg and Si, is best derived by other means.

Mantle peridotites from a variety of tectonic settings (e.g., xenolith and massifs, Canil 2004) have rather constant SiO₂ contents, at 45.4 ± 0.3 wt. %, as a function of their Mg#, $\text{Mg}/[\text{Mg} + \text{Fe}^{2+}]$. The Mg# is a proxy for mantle differentiation, either by partial melt extraction/addition (e.g., Herzberg 2004) or by mixing of mineralogical heterogeneities (e.g. Spray 1989, O'Neill and Palme 1998). Regardless of the mechanism, the constancy of SiO₂ in peridotites permits estimates of mantle Mg/Si, provided that the MgO abundance is known. The observation that the Mg#s of peridotites rarely extend below 0.89 and their FeO contents are uniform (8.1 ± 0.1 wt. %) implies an MgO content of ~ 36.8 wt. %. This translates into an Mg/Si ratio of 1.21 ± 0.05 , exceeding those of all known chondrites (0.73–1.07; Wasson and Kallemeyn 1988); indeed, the superchondritic nature of the Earth's upper mantle is well-established (cf. Jagoutz et al. 1979, Ringwood 1979). Whether these chemical characteristics apply to the entire mantle is uncertain, as the sampled peridotites are all derived from the mantle lithosphere. Although some record geobarometric pressures up to ~ 7 – 8 GPa (e.g., Boyd 1989), the majority are spinel lherzolites with equilibration pressures of ~ 1 – 2 GPa (30–60 km; Walter 2003), casting doubt over whether these samples are representative of the Earth's convective mantle.

Inversion of the composition of mid-ocean ridge basalt (MORB) to calculate that of its source mantle can yield complementary estimates to peridotites. Since much of the upper mantle undergoes melting at mid-ocean ridges over time ($\sim 10\%/100$ Myr by volume, Matthews et al. 2016), the products (basaltic crust and harzburgitic residue) are, together, thought to be representative of the composition of the upper mantle (Ringwood 1979). The inferred MORB-source composition, termed "pyrolite" (or DMM; Workman and Hart 2005), is compositionally akin to sampled peridotites. However, the convecting upper mantle is not necessarily a good proxy for the BSE, because there is no mandate for it to have

chondritic refractory lithophile element ratios. Indeed, the composition of the convecting upper mantle may be complementary to other, potentially unsampled reservoirs within the mantle (see section 5). In any case, the Mg/Si of pyrolite/DMM is even more superchondritic (~ 1.27 ; Ringwood 1979, Workman and Hart 2005) than that of the BSE as estimated from peridotites, assuming a chondritic Ca/Al ratio (~ 1.21 Palme and O'Neill (2014)). The following, not mutually exclusive, possibilities for the superchondritic Mg/Si of the Earth's upper mantle are:

- i) non-chondritic Mg/Si of Earth's building blocks, inherited from its accretion
- ii) sequestration of some fraction of the Si into the core
- iii) chemical differences between the Mg/Si ratio of the Earth's upper and lower mantles.

Arguments for each of the three scenarios, the first two of which do not require a difference in the bulk compositions of the upper and lower mantle, are examined in more detail below.

2.2. Chemical and isotopic fractionation during Earth's accretion

Cosmochemically, the Earth falls at the end of a correlation between Fe/Si and Fe/Mg in chondrites (Yoshizaki and McDonough 2021, Khan et al. 2022, ; Fig. 1). However, there is no a priori reason to expect that the Earth should lie on this line, owing to its non-chondritic nature in a number of element and isotope ratios (e.g., ^{142}Nd ; Frossard et al. 2022). Nevertheless, it is reasonable to expect that the Earth's composition lies on an *extension* of the chemical fractionation trends defined by chondrites, even if there is no one body that bears this composition. Such chemical variation could arise during condensation of the solar nebula (cf. Larimer 1967), where the Mg/Si ratio of chondrites depends on the relative proportions of olivine (Mg_2SiO_4) and orthopyroxene (MgSiO_3); with enstatite chondrites (EC) having accumulated relatively more of the latter, resulting in their low Mg/Si ratios (~ 0.73 ; Wasson and Kallemeyn 1988). Their key condensation reactions are given by:



where g and s refer to gas and solid phase, respectively.

For a solar composition, eq. 1 proceeds to the right at higher temperatures (~ 1380 K at 10^{-4} bar) than does eq. 2 (~ 1300 K at 10^{-4} bar), resulting in an increase in the partial pressures (p), $p\text{SiO}/p\text{Mg}$, of the residual gas sufficient to promote condensation of MgSiO_3 (e.g., Yoneda and Grossman 1995). It follows that a simple model to explain the superchondritic Mg/Si ratio of the Earth (should it reflect that of the BSE) would be that it accreted material that had preferentially accumulated olivine relative to orthopyroxene (e.g., the chemical complement to enstatite chondrites).

Support for this scenario comes from Si isotopes (expressed as $\delta^{30}\text{Si}$; the $^{30}\text{Si}/^{28}\text{Si}$ deviation from that of the NBS-28 standard), in which the bulk silicate Earth (and Moon) have $\delta^{30}\text{Si}$ that is distinctly heavier (-0.29 ± 0.03 ‰) than any chondrite. Carbonaceous and some ordinary chondrites span a range from about -0.7 ‰ (EH) to about -0.4 ‰ (Fitoussi et al. 2009). The $\delta^{30}\text{Si}$ is positively correlated with the Mg/Si ratio of the chondrite parent body or planet (including the Earth, although heavily weighted by the ECs; Fitoussi et al. 2009), while the $\delta^{26}\text{Mg}$ isotope ratio remains constant over the same Mg/Si

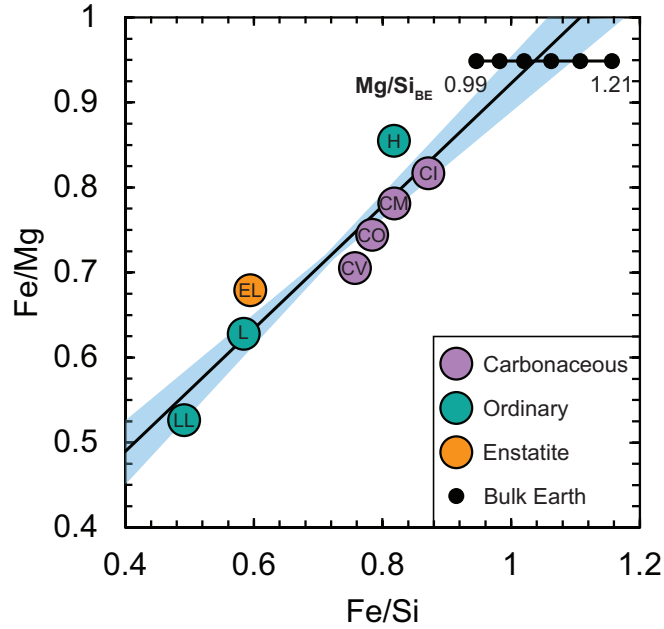


Figure 1

Distribution of molar Fe/Mg and Fe/Si within chondritic meteorites; purple = carbonaceous, aquamarine = ordinary, orange = enstatite (data from Wasson and Kallemeyn, 1988) and for the bulk Earth (BE) for varying Mg/Si ratios from BSE-like, 1.21, as inferred from upper mantle peridotites (Palme and O'Neill 2014), to 0.99, corresponding to a lower mantle Mg/Si of 0.9 (i.e., entirely bridgmanitic), or a core Si content of 10 wt. %.

interval (Dauphas et al. 2015). These observations can be understood in terms of equilibrium isotope fractionation between olivine and orthopyroxene and Mg- and Si-bearing gas species (reactions 1, 2; Dauphas et al. 2015). The corresponding isotopic fractionation factor, $\Delta^{30}\text{Si}_{\text{ol-gas}} = \delta^{30}\text{Si}_{\text{ol}} - \delta^{30}\text{Si}_{\text{gas}} \simeq 4 \times 10^6 / T^2$, where T is temperature, while much of the Mg is condensed into forsterite (compared to only 50% of the Si) by 1300 K, meaning Mg isotopes remain essentially unfractionated from the nebular gas. Subtraction of an isotopically heavy, olivine-rich component would therefore simultaneously explain the chondritic $\delta^{26}\text{Mg}$ and the heavy $\delta^{30}\text{Si}$ composition of the BSE (Dauphas et al. 2015).

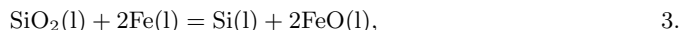
2.3. Evidence for Si in the core

If the Earth lies on the nebular trend (Fig. 1; Dauphas et al. 2015), then the inferred fraction of Si in the core (assuming a whole-mantle composition with Mg/Si = 1.21) is given by the intersection of the Mg/Si of the bulk Earth with that of the chondrite trend. However, the uncertainty on the trend is such that a wide range of Mg/Si ratios in the bulk Earth are permissible; Fig. 1 indicates a best-fit value of Mg/Si = 1.10 ± 0.06 and hence $\sim 4.5 \pm 2.5$ wt % Si in the core, indistinguishable from the $3.6^{+6.0}_{-3.6}$ wt. % determined by Dauphas et al. (2015). A similar exercise was undertaken by O'Neill and Palme (1998)

on the basis of Mg/Si *vs.* Al/Si ratios, indicating that the Earth would intersect the CC trend (which has constant Mg/Si = 1.06) with 5 wt. % Si in the core. If correct, then this would suggest that, chemically, the material that accreted to form the Earth had affinities to CCs (Witt-Eickschen et al. 2009, Sossi et al. 2018).

Independent indications for the siderophile behaviour of Si comes from *i)* metal-silicate partitioning and *ii)* the light element content of the core that satisfies its geophysical properties, in particular the ~10% density deficit relative to Fe-Ni alloy at the same *P-T* (Badro et al. 2014, Hirose et al. 2021), although SC-REM (Kemper et al. 2023, section 3) indicates a denser outer core, which would act to reduce the aforementioned density deficit.

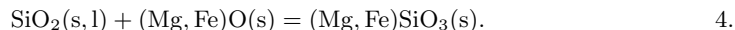
Silicon enters the core via the equilibrium:



where l refers to liquid phase, implying that incorporation of Si into the core oxidises Fe into FeO. Reaction (3) proceeds to the right with increasing temperature and has only a weak dependence on pressure, as shown by free energy- and experimental data (O'Neill et al. 1998, Ricolleau et al. 2011). The corollary is that, because condensation of Si and Fe in the solar nebula took place at low temperatures (~1400 K at 10⁻⁴ bar), all Si condenses as olivine and orthopyroxene (eqs. 1 and 2), and hence would have initially been present in the Earth as an SiO₂ component. Insofar as this assumption is reasonable, eq. (3) implies that, for the 8.1 wt.% FeO in the Earth's mantle (in a closed system) 3.5 wt. % Si is required in its core. This value coincides with that needed for the bulk Earth to intersect the carbonaceous chondrite trend in Mg/Si-Si isotope space (Dauphas et al. 2015, see also Fig. 1), and falls within the range predicted by heterogeneous accretion simulations of the Earth (Ricolleau et al. 2011). Geophysical arguments also favour <4.5 wt. % Si in the core on the basis of elastic properties of binary Fe-X mixtures (Badro et al. 2014, Umemoto and Hirose 2020) determined via *ab-initio* calculations and their fit to PREM, particularly to the density and V_P of the core (see Hirose et al. 2021, for a recent summary). This number may need revision, however, in light of new models of the Earth's seismic profile (e.g., SC-REM, Kemper et al. 2023, section 3) or the properties of metals at high pressures and temperatures.

2.4. Geochemical constraints on differences in composition between the upper and lower mantle

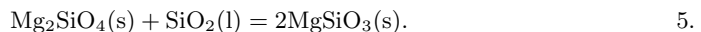
2.4.1. SiO₂ exsolution from the core. While present-day seismic and geochemical constraints appear to favour ~4 wt. % Si in the core (bulk Earth Mg/Si ~1.11), its initial budget may have been markedly higher, owing to its secular cooling. Because the equilibrium constant of eq. (3) increases with increasing temperature, cooling would have led to the exsolution of SiO₂ (Hirose et al. 2017, Helffrich et al. 2018, though see Huang et al. (2019)). This excess SiO₂, hypothetically, could be stored in the lower mantle (option *iii*), should subsequent convection failed to have chemically homogenise the mantle (see also section 5). On contact with the lower mantle, it would react with ferropericlaase to produce additional bridgmanite;



The amount of SiO₂ exsolved cannot be uniquely constrained, as the initial conditions under which the core initially formed are unknown. Qualitatively, SiO₂ formation would

require reduction of FeO initially in the mantle to Fe (eq. 3), which implies the core would have had to have formed under more oxidised conditions (i.e., higher FeO in the mantle) than observed today. As such, the process is self-limiting, because higher FeO hinders Si dissolution into core-forming metal. Alternatively, SiO₂ may enter the lower mantle mechanically as stishovite (i.e., without reacting with ferropericlasite according to eq. 3) due to convective instability of an SiO₂-enriched layer atop the core-mantle boundary Helffrich et al. (2018). Small stishovitic regions may float into the (lower) mantle, consistent with the detection of strong seismic scatterers (Kaneshima and Helffrich 2010). Partial melting products of the convecting mantle through time provide an independent record of the compositional differences, if any, between the lower- and upper mantle.

2.4.2. The message from igneous rocks. The major element compositions of igneous rocks reflect those of their mantle sources. Because partial melts of peridotite are saturated in both olivine and orthopyroxene at low pressures ($\sim 0\text{--}4$ GPa), their silica activities (a_{SiO_2}) are buffered by the reaction:



Owing to the partial molar volume change (ΔV) of reaction (5), liquids become poorer in silica (i.e., lower a_{SiO_2}) as pressure increases. The SiO₂ contents of primitive mid-ocean ridge basalt (MORB) glasses (SiO₂ ~ 49 wt.%; Jenner and O'Neill 2012) are consistent with their derivation from 10–15% partial melting of an upper mantle with ~ 45 wt. % SiO₂ and ~ 37 wt. % MgO₂ (i.e., Mg/Si ~ 1.22 ; Baker and Stolper 1994).

At higher pressures (above 4 GPa), near-solidus partial melts of peridotite are no longer saturated in orthopyroxene (Walter 1998), meaning eq. (5) does not buffer a_{SiO_2} . Experiments show that SiO₂ contents of partial melts of pyrolitic mantle (Mg/Si ~ 1.24) have a narrow range; 46–47.5 wt % for $3 < P(\text{GPa}) < 7$ at high melt fractions, $25 < F(\%) < 45$ (Walter 1998, Fig. 2). Although modern plume-derived magmas may be sourced from the lower mantle, they form by $\sim 5 - 15$ % melting (Herzberg and Asimow 2015), over which SiO₂ varies significantly with F (Fig. 2). This, together with their heterogeneous sources, renders them unsuitable for determining the mean composition of the convecting lower mantle. Komatiites are more amenable to this task, as they formed by higher degrees ($\sim 25 - 45$ %) of partial melting of near-primitive mantle (e.g. Nisbet et al. 1993, Sossi et al. 2016).

Most komatiite primary melts have between 45.5 – 49 wt % SiO₂ (Sossi et al. 2016), whereas the Comondale lavas (Wilson 2019) have ~ 50 wt. % SiO₂ and contain primary orthopyroxene, suggesting silica enrichment at the locus of melt extraction. Assuming a first-order linear relationship between the SiO₂ contents of silicate liquids and mantle Mg/Si, this permits a maximum Si enrichment over the BSE value of 5–10 %. If representative of the lower mantle, it would imply a $(\text{Mg/Si})_{\text{LM}} \sim 1.12$. Considering that the lower mantle comprises ~ 70 % of the total mantle mass, the corresponding $(\text{Mg/Si})_{\text{BSE}}$ would be ~ 1.15 .

A complementary view on mantle composition is proffered by RLEs. Most komatiite suites have initial $^{176}\text{Lu}/^{177}\text{Hf}$ and $^{147}\text{Sm}/^{144}\text{Nd}$ compositions that lie on a line between the chondritic uniform reservoir (CHUR; 0.034 and 0.192, respectively) and DMM (0.039 and 0.216, respectively) (Puchtel et al. 2022, and references therein). That komatiite source regions can be reproduced by mixing between a DMM-like source residing in the upper mantle on the one hand, and a chondritic reservoir on the other implies that there are no large-scale differences in the compositions of the (convecting) upper- and lower mantle (see section 5.3), at least with respect to RLEs. Some komatiites from the Kaapvaal craton

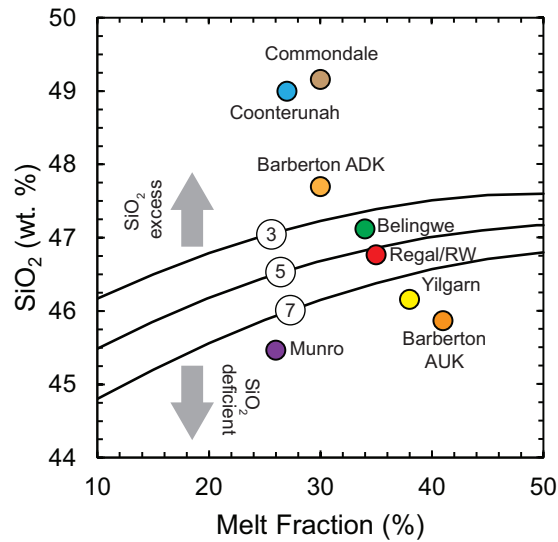


Figure 2

SiO₂ contents of komatiite parental melts (Sossi et al. 2016, Wilson 2019) as a function of their melt fraction (expressed in %), overlain by curves of silicate liquids produced in partial melting experiments of West Kettle River peridotite (Mg/Si = 1.24) at different pressures; 3, 5 and 7 GPa (circles; Walter 1998). The majority of komatiite liquids are in equilibrium with their sources between ~3 and 7 GPa (cf. Sossi et al. 2016), and hence their compositions should lie within uncertainty of these curves. Departures therefrom may indicate silica deficiency or excess in their mantle sources, which are, in turn, relatively insensitive to uncertainties in melt fraction.

diverge from this array, a feature suggested to reflect variable bridgmanite/ferropericlasite ratios in their sources (Puchtel et al. 2022).

Walter et al. (2004) proposed that the marginally superchondritic Ca/Al ratio of the accessible mantle could arise from a ~10-20 % enrichment of bridgmanite in the lower mantle (see also Jackson et al. 2014). However, as bridgmanite favours Hf ($D_{br/melt} = 2$) over Lu ($D_{br/melt} = 0.2$) (Walter et al. 2004, Liebske et al. 2005), this would produce subchondritic ¹⁷⁶Lu/¹⁷⁷Hf in hypothetical lower mantle sources, which are not observed in any komatiites. Because the exchange coefficient, $K_{D,br/melt}^{Mg/Si}$ approaches unity as $(Mg/Si)_{liquid=BSE}$ tends to 1, Si enrichment by bridgmanite accumulation becomes ineffective for hypothetical ‘chondritic’ BSE compositions, and the observed value of $(Mg/Si)_{DMM} \sim 1.25$ cannot be achieved (Liebske et al. 2005). Indeed, 13 % removal of a 96:4 br:ca-pv assemblage (the maximum permitted to retain chondritic Ca/Sc and Ca/Yb within ± 10 %) would only increase the Mg/Si ratio of the residual upper mantle by ~2.5 % (Liebske et al. 2005).

Chemical arguments suggest minimal preferential br/ca-pv accumulation in the lower mantle relative to the upper mantle, so as to maintain near-chondritic RLE ratios and Hf-Nd isotope compositions in ultramafic rocks. Nevertheless, these constraints are based on experiments near ~25 GPa, whereas element partitioning at higher pressures may differ. The observed SiO₂ contents of komatiites are also consistent with upper mantle-like Mg/Si ratios (within 10 % relative), placing limits on the Mg/Si ratio of the lower mantle to ≥ 1.12 .

3. Lower mantle composition and thermal state: a geophysical perspective

Seismological constraints on Earth’s mantle composition typically derive from a comparison of radial seismic models such as the preliminary reference earth model (Dziewonski and Anderson 1981) with laboratory measurements of the elastic properties of the relevant minerals at the appropriate pressures and temperatures (e.g., Ita and Stixrude 1992, Jackson 1998, Ganguly et al. 2009, Murakami et al. 2012). Because of the inherent limitations in qualitative comparisons, however, recent studies have sought to infer compositional and thermal parameters directly from seismic models and/or data based on geophysical properties that are computed using parameterized phase diagram approaches (e.g., da Silva et al. 2000, Trampert et al. 2004, Cammarano et al. 2005) or thermodynamically self-consistent methods (e.g., Bina 1998, Ricard et al. 2005, Khan et al. 2006, Matas et al. 2007, Cobden et al. 2009, Afonso et al. 2013, Fullea et al. 2021, Kemper et al. 2023). The latter methods, which oftentimes rely on Gibbs free-energy minimisation, allow for the prediction of seismic properties as a function of pressure, temperature, and bulk composition from thermodynamic data, as a consequence of the availability of comprehensive thermodynamic data bases (e.g., Fabrichnaya et al. 2004, Stixrude and Lithgow-Bertelloni 2011a, 2005a, 2021, Khan et al. 2006, Piazzoni et al. 2007).

Several strategies exist for computing seismic properties from thermodynamic data, some of which rely on precomputed phase diagrams corresponding to fixed compositions and geotherms that are augmented with an external database of physical properties as implemented in, e.g., the Subduction factory (Hacker and Abers 2004, Abers and Hacker 2016) and Burnman (Myhill et al. 2023). Alternatively, Gibbs free energy minimisation (Gfrem) methods allow for computing seismic properties dynamically (“on the fly”) as a function of composition, temperature, and pressure as implemented in e.g., *Perple_X* (Connolly 2009), *HeFesto* (Stixrude and Lithgow-Bertelloni 2011a), *MMA-EoS* (Chust et al. 2017), and *PheMgp* (Zunino et al. 2011).

The immediate advantage of this approach is that size and location of discontinuities in seismic properties associated with pressure-induced mineralogical phase changes are modeled in a physically-realistic manner, as their variations depend on composition, pressure, and temperature as illustrated in Figure 3 for three mantle-relevant compositions. Another virtue of Gfrem over parameterised approaches is its versatility within an inverse framework, wherein thermo-chemical parameters are sought constrained directly from geophysical data (e.g., Khan 2016).

3.1. Mineralogical predictions

The class of models with a homogeneous mantle whose composition is typified by varying Mg/Si ratios, as illustrated in Fig. 3 reveals key, first-order trends in the expected mineralogy of the lower mantle along an isentrope. Relative to the upper mantle, its phase assemblage is relatively simple; it comprises predominantly bridgmanite (br; general formula ABO_3 in the perovskite structure) and ferropericlase (fp; typically $Mg_{1-x}Fe_xO$ in the rock-salt B1 structure), with the $br/[fp+br]$ ratio being a negative function of Mg/Si. For a pyrolitic Mg/Si (=1.27), $br/[fp+br] \sim 0.8$, whereas for a ‘cosmic’ Mg/Si of 1, it increases to ~ 0.95 .

This dependence results from the near-absence of SiO_2 in fp (~ 1 wt.%; Frost and Myhill 2016), which is otherwise dominated by MgO and FeO, making bridgmanite the overwhelming host of Si in the lower mantle. Bridgmanite is predominantly composed of

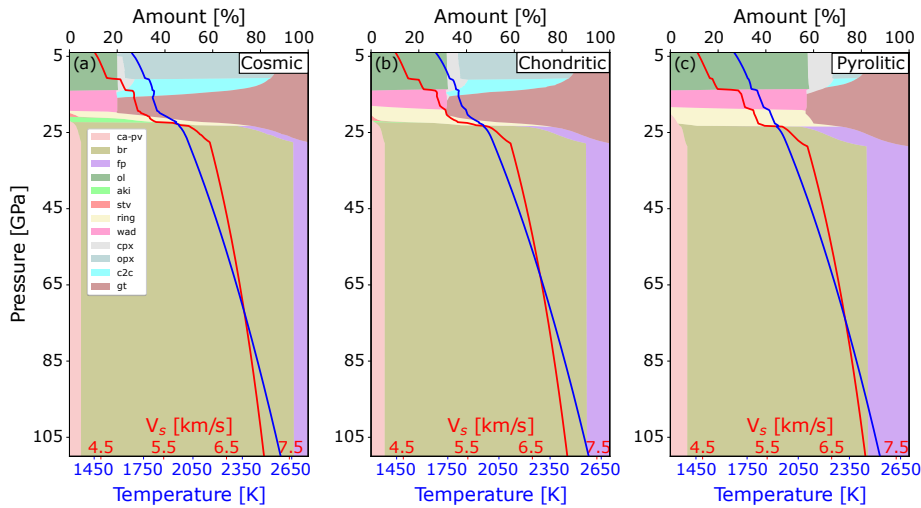
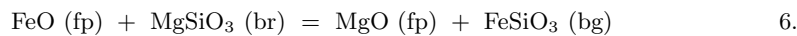


Figure 3

Illustration of variations in phase proportions, isotropic seismic shear-wave speed (V_S), and mantle isentropes (computed for a temperature of 1648 K at 80 km depth) in the pressure range 5–110 GPa for three different hypothetical mantle compositions based on the equilibrium model: a) cosmic ($Mg/Si \sim 1$), b) chondritic ($Mg/Si \sim 1.1$), and c) pyrolite ($Mg/Si \sim 1.27$) in the CFMASNa system (comprising oxides of the elements CaO-FeO-MgO-Al₂O₃-SiO₂-Na₂O). Phases are: olivine (ol), orthopyroxene (opx), clinopyroxene (cpx), pl (plagioclase), coe (coesite), stv (stishovite), high-pressure Mg-rich cpx (C2/c), garnet (gt), wadsleyite (wad), ringwoodite (ring), akimotoite (aki), calcium silicate perovskite (ca-pv), ferropericlase (fp), bridgemanite (br), and calcium ferrite (cf). The seismic discontinuities are: ol→wads (“410”), wads→ring (“520”), and ring→br+fp (“660”).

MgSiO₃, with ~ 10 mol % FeSiO₃, FeAlO₃ and AlAlO₃ components (Frost and Myhill 2016). Calcium-perovskite, whose modal abundance (~ 5 wt. %) is constrained by the content of Ca, an RLE, of the lower mantle, has a composition close to end-member CaSiO₃. The ionic radius of Ca makes ca-pv the prevailing host of large-ion lithophile elements, as well as rare-earth elements, U and Th, in the lower mantle (Corgne et al. 2005).

Consequently, the major elemental exchange reaction occurring in the lower mantle is among Mg and Fe²⁺ between br and fp, given by:



and, at equilibrium

$$K_D^{Fe-Mg} = \frac{X_{FeSiO_3}^{bg} X_{MgO}^{fp}}{X_{MgSiO_3}^{bg} X_{FeO}^{fp}} \quad 7.$$

where X pertains to the mole fraction. In eq. (6), all Fe is presumed to be ferrous, and experimental data in Al-free systems indicate a near-constant K_D of ~0.2 between 25 and ~70 GPa, before decreasing to ~0.05 by 100 GPa (Piet et al. 2016), likely owing to the high-spin to low-spin transition of Fe²⁺ in fp (Badro 2014b). In Al-bearing systems, the substitution FeAlO₃ (where ferric iron resides on the dodecahedral A-site) is energetically favoured, resulting in an increase in the apparent K_D to ~0.5 - 0.8 (Frost and Myhill 2016,

Piet et al. 2016, Huang et al. 2021). Therefore, at a given pressure and temperature, the elastic properties of br and fp depend not only on X_{FeO} , but on its distribution between the two phases, the Fe^{3+}/Fe^{2+} in bg, and the extent of the spin transformation in ferrous iron in both fp and bg.

3.2. Methods for geophysical inversion of lower mantle composition

The interpretation of seismological models for the Earth’s lower mantle in terms of chemical composition and temperature is sensitive both to the details of the methodology employed and also to uncertainties in key thermoelastic parameters of lower mantle minerals. As a consequence, interpretations of the composition and thermal state of Earth’s lower mantle have varied widely. More specifically, these discrepancies arise from a number of inconsistencies, including 1) the choice of mineral elastic parameters and the method by which these are extrapolated to lower mantle conditions; 2) the choice of chemical system; 3) the consideration of bulk sound velocities only; 4) the nature of the geophysical data or model(s) against which the thermochemical models are compared, particularly in view of the fact that radial seismic reference models lack uncertainties; 5) incomplete consideration of uncertainties associated with thermoelastic parameters of relevant minerals; and 6) the nature of the conversion from thermo-chemical to seismic parameters. Moreover, arguments have been advanced supporting the case for mantle material consisting of a mechanical mixture (MM) rather than an equilibrium assemblage (EA) of minerals on the grounds that the former provides a better fit to the seismic wave speeds of radial reference models in the transition zone structure (Xu et al. 2008). However, the arguments put forward by Xu et al. (2008) in favour of MM over EA are purely qualitative (see also discussion in Bina and Helffrich 2014). Quantitative analysis, meanwhile, indicates (e.g., Munch et al. 2020, Bissig et al. 2022a) that regional- and global-scale seismic waveform data are matched to a similar extent by either parameterisation, although chemical equilibration appears to be less prevalent underneath stable cratonic regions, yet neither of them are capable of completely matching the seismic wave velocity gradients in the mantle transition zone (Bissig et al. 2022b).

Exemplary of the class of studies that rely on a model of physical properties supplemented with an account of phase equilibria based on a graphical summary of experimental data is that of Cammarano et al. (2005). Mantle mineralogy is fixed on the basis of a pyrolitic composition and a specified geotherm. Physical properties in the form of bulk and shear moduli, their pressure and temperature derivatives, and thermal expansion are varied separately within specified bounds. Because of the restrictions imposed by the parameterisation, their ability to fit the geophysical data (global P- and S-wave travel times) is severely limited, leading to the suggestion that other compositions in the lower mantle, possibly in combination with a superadiabatic thermal gradient, are needed.

Representative of studies that rely on thermodynamic self-consistency is that of Matas et al. (2007). While composition and geotherm are varied (the former also with depth), and, in turn, mineralogy and bulk seismic properties, inversion is restricted to fitting a radial seismic velocity profile (AK135) with unspecified uncertainties. The importance of this study lies in the incorporation of model parameter uncertainties in the inversion that impact the elastic properties of the major lower-mantle minerals.

In addition to considering the uncertainties associated with the elastic parameters, Cobden et al. (2009) also explored the influence of the assumed equation-of-state in modeling

lower-mantle composition and temperature. Based on matching radial reference profiles, Cobden et al. (2009) found that a superadiabatic temperature gradient in combination with a lower-mantle composition that becomes increasingly enriched in a basaltic component with depth provide the best results, but also conclude that a lower mantle consisting of adiabatic pyrolite cannot be ruled out completely.

A more comprehensive approach is to combine the different pieces, i.e., data and results from mineral physics experiments, geochemical and petrological analyses of mantle minerals, and geophysical inverse calculations, to directly transform geophysical data into the mantle composition and thermal state. This approach is illustrated in e.g., Khan et al. (2006) and Khan et al. (2008), who inverted long-period electromagnetic sounding data and global seismic travel-time data for Earth's mantle composition and thermal state, respectively. The results generally agreed with earlier geophysically-derived conductivity and seismic velocity models and indicated most probable core-mantle-boundary temperatures of around 3200 K, and bulk Earth Mg/Si ratios of 1.05–1.15, intermediate between a cosmic and a chondritic composition.

Common to these studies, however, are limitations in assessing the uncertainties in computed geophysical properties. Parameterised phase diagram approaches, for example, are only able to consider the uncertainty in the elastic properties of the minerals and ignore the uncertainty associated with the identity and the compositions of the stable minerals, thereby underestimating the overall uncertainty. Generally, uncertainties of 0.5–1%, 1–2%, and 2–4% in mantle density, P wave speed, and S wave speed, respectively, are found (Kuskov and Fabrichnaya 1994, Connolly and Kerrick 2002, Kennett and Jackson 2009, Connolly and Khan 2016). The thermodynamic model precludes consideration of redox effects that may be important if native or ferric iron are present in the lower mantle. Finally, the thermodynamic model also precludes consideration of minor phases and components such as water and melt due to lack of thermodynamic data, although these are not expected to be important in the lower mantle with the exception of maybe D'' , which is beyond the scope of this study.

Table 1 summarises a selection of studies in terms of estimates of lower mantle composition and thermal state and other modeling details. To further constrain the wide compositional range, integration of seismic modelling with experimental mineral physics measurements of relevant materials at the pressure and temperature conditions of the lower mantle is required.

4. Experimental mineral physics: constraints from elasticity

4.1. Experimental considerations

A first-order means toward constraining the mineralogy and, in turn, the chemistry of the lower mantle is to directly compare seismic reference models with mineral properties determined experimentally under relevant high-pressure and high-temperature conditions (section 3). Significant technical progress over the past few decades in *in situ* high-pressure sound velocity measurements using Brillouin light scattering (BLS) combined with a diamond anvil cell (DAC) have enabled the determination of longitudinal sound and transverse wave speeds (hereinafter V_P and V_S) of mantle phases under lower mantle pressures (~ 25 – 135 GPa). The Earth's lower mantle largely consists of two minerals bridgmanite (br) and ferropericlase (fp) (Irifune et al. 2010) and, depending on composition, minor amounts (~ 7 vol%) of calcium-perovskite (ca-pv) (see Figure 3). Thus, V_P and V_S profiles of the

lower mantle can, to a first approximation, be constructed from V_P and V_S measurements of these two minerals. This extends earlier inferences that were based on extrapolation of measurements obtained at low pressure (see Murakami 2013, for a review). Here, we review the status of high-pressure V_P and V_S measurements of bridgmanite and ferropericlase with a special emphasis on V_S velocities, which were primarily obtained by BLS within the lower mantle pressure range, and discuss mineralogical models of the lower mantle.

The BLS technique is based on the inelastic light scattering related to the photon-phonon interaction between the probe laser and thermally-generated phonon in a sample. The V_P and V_S of a sample in a DAC placed in symmetric platelet geometry is obtained from the shift in frequency ($\Delta\omega$) according to:

$$V_i = \frac{\Delta\omega_i\lambda}{2\sin(\theta/2)}, \quad 8.$$

where λ is the laser wavelength, θ is the external scattering angle, and i denotes either shear or longitudinal mode. Since the BLS technique in a DAC is based on the scattered light transmitted through a sample, as long as the sample is sufficiently transparent, a combination of the BLS technique and DAC serves as an effective method to determine V_P and V_S *in situ* under extremely high-pressure conditions (Murakami et al. 2009a).

With this method, V_P and V_S data of materials making up Earth’s interior have been extensively collected from single-crystal samples since the 1970s (e.g., Weidner et al. 1975). However, due to technical issues (see e.g., Murakami 2013, for more discussion), most of the results from single-crystal measurements were limited to relatively low pressures (~ 30 – 40 GPa), which are insufficient to constrain the mineralogy of the entire lower mantle. For example, Kurnosov et al. (2017) report the sound velocity of single-crystal Fe- and Al-bearing bridgmanite up to ~ 40 GPa, which was found to be compatible with a pyrolitic (Mg/Si ≈ 1.27) uppermost lower mantle consisting of br ~ 80 vol% based on comparison with PREM. However, extrapolating their velocity profile to higher pressures results in large deviations from PREM at depths below 1200 km, indicative of significant uncertainties with this procedure (Lin et al. 2018). Recent experimental efforts by Criniti et al. (2021) and Fu et al. (2023) on single-crystal V_P and V_S measurements of lower mantle phases have extended pressures to ~ 80 GPa. Criniti et al. (2021) reported V_P and V_S measurements of pure MgSiO₃ bridgmanite to 79 GPa by carefully aligning the orientation of the diamond anvils to observe both V_P and V_S of bridgmanite using the BLS technique. Their studies also support a model of the lower mantle made up of pyrolite (to mid-lower mantle depths). Comparison of Criniti et al. (2021) and Kurnosov et al. (2017) indicates that 10 mol% of the FeAlO₃ component (in which Fe is ferric) in bridgmanite results in a decrease of K_{S0} , G_0 , and K' , while increasing G' , where the former two are the bulk adiabatic and shear modulus at zero pressure and the latter two refer to bulk adiabatic and shear modulus pressure derivative. This result is counter to recent measurements on single-crystal Mg_{0.88}Fe_{0.1}Al_{0.14}Si_{0.90}O₃ bridgmanite by Fu et al. (2023) that were performed up to 82 GPa using BLS in combination with an impulsive stimulated light scattering method. Fu et al. (2023) showed that the incorporation of Al and Fe in bridgmanite reduces G_0 and increases G' , while the effect on K_{S0} and K' appears to be insignificant. The results of Fu et al. (2023) are compatible with a bridgmanite-enriched lower mantle consisting of up to 89 vol% br.

The first V_S data of bridgmanite determined under lower-mantle pressure conditions were obtained at pressures up to 96 GPa using polycrystalline MgSiO₃ bridgmanite synthesized *in situ* at the pressure-temperature conditions of the lower mantle in a laser-heated

DAC. This result allows for a significant extension of the pressure limit of BLS measurements (Murakami et al. 2007a). Since then, V_P and V_S of polycrystalline silicate samples have successfully been measured to pressures of ~ 170 GPa (Murakami et al. 2007b). With this newly-developed high-pressure BLS method, all subsequent V_S measurements of polycrystalline br, including Al-bearing and Fe-bearing bridgmanite (Murakami et al. 2012, Mashino et al. 2020), were carried out at pressures equivalent of those covering the lower mantle. The measured transverse elastic properties (shear modulus and its pressure derivative) of both bridgmanite and ferropericlase at lower-mantle pressures are summarized in Figure 4.

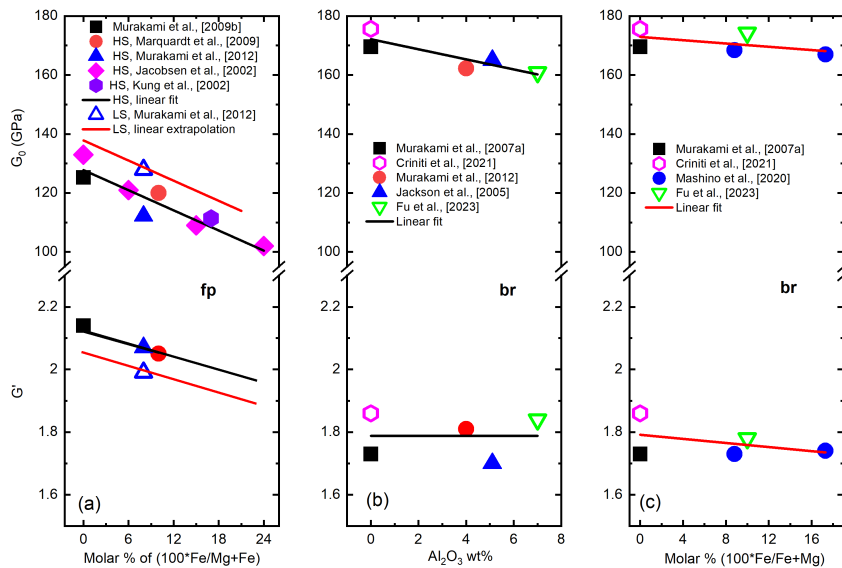


Figure 4

Summary of recent experimental mineral physics measurements of shear modulus (G_0) and its pressure derivative (G') as a function of composition. Variation of G_0 and G' with respect to Fe^{2+} in ferropericlase (fp) (a); Al_2O_3 in MgSiO_3 (bridgmanite, br) (b); and Fe^{2+} in MgSiO_3 (br) (c). Solid black and red lines represent the fitted linear dependence of G_0 and G' with pressure. Note that the low-spin state (red line) assumes the same linear dependence as the high-spin state of fp.

4.2. Constructing lower mantle seismic profiles from experimental data

The longitudinal sound and transverse elastic properties of both br and fp obtained at lower-mantle pressures using the BLS method are summarized in Table 2. Here, we focus on a lower-mantle mineralogical model constructed by combining all the data. In the modelling procedure, shear modulus (G_0) and its pressure derivative (G') play an essential role, where G' is obtained from fitting high-pressure shear modulus (G) as a function of finite strain (ϵ). Moreover, to extract the consistent elastic properties of the lower mantle phases over the entire lower-mantle pressure range, it is important that all data are fitted using a single

formalism. Accordingly, we employ the third-order Eulerian finite-strain equation (Stixrude and Lithgow-Bertelloni 2005b) to refit the existing polycrystalline data, given that improper truncation of the finite-strain equation could result in up to $\sim 10\%$ -difference in estimated G' values (e.g., Myhill et al. 2023, Fu et al. 2023):

$$G = (1 + 2\epsilon)^{\frac{5}{2}} G_0 + (3K_{S0}G' - 5G_0)\epsilon + (12K_{S0}G' - 48K_{S0} - 28G_0 + 9K_{S0}K')\epsilon^2 \quad 9.$$

with

$$\epsilon = \frac{1}{2} \left[\left(\frac{\rho}{\rho_0} \right)^{\frac{2}{3}} - 1 \right] \quad 10.$$

where ρ_0 and ρ are the sample density at ambient conditions and at high pressure estimated from X-Ray Diffraction (XRD) measurements, respectively, while G is obtained from the BLS measurements. Incidentally, the same formalism is employed in section 3 above. The refitted G_0 and G' values are summarized in Table 2. The thermal pressure (P_{th}) and temperature effect on G (G_{th}) and K (K_{th}) is incorporated through the Mie-Grüneisen-Debye equation-of-state (Stixrude and Lithgow-Bertelloni 2005b) using the following expressions:

$$P_{\text{th}}(V, T) = \frac{\gamma_0 \Delta U}{V}, \quad K_{\text{th}}(V, T) = (\gamma_0 + 1 - q) \frac{\gamma_0 \Delta U}{V} - \gamma_0^2 \frac{\Delta(C_V T)}{V} \quad \text{and} \quad G_{\text{th}}(V, T) = \frac{-\eta_{S0}}{V} \quad 11.$$

where, ΔU is the internal energy at room temperature, γ_0 is the Grüneisen parameter, C_V is the specific heat at constant volume, q is the logarithmic derivative of the Grüneisen parameter with respect to volume, and η_{S0} is the shear-dependent part of the finite-strain generalization of the Grüneisen parameter, V is volume, and Δ refers to change in parameter(s). After evaluating thermoelastic parameters of each mineral at corresponding lower mantle pressure and temperature, they are combined to estimate V_P and V_S of the multiphase assemblage using the Voigt-Reuss-Hill average.

The effect of Fe in ferropericlase on G_0 and G' in the high-spin (HS) and low-spin (LS) states and the effect of Fe and Al_2O_3 in bridgmanite (Badro 2014a) on G_0 and G' are shown in Figure 4. Since there is only a single V_P and V_S measurement of ferropericlase (8 mol% Fe) in the LS state (Murakami et al. 2012), the effect of iron content on the elasticity of ferropericlase in the low-spin state is estimated assuming that the change in trend is similar to that in the high-spin state. The effect of the spin transition on the elasticity of bridgmanite is neglected as it remains unclear as to whether bridgmanite is affected at all (Badro 2014a, Kurnosov et al. 2017, Mashino et al. 2020).

The resulting compositional effect on the shear modulus and its pressure derivative of bridgmanite is as follows:

$$G_0 = 172.92 - 1.71 \times \text{Al}_2\text{O}_3 - 27.83 \times \frac{\text{Fe}}{\text{Fe} + \text{Mg}} \quad 12.$$

$$G' = 1.79 + 8.169 \times 10^{-5} \times \text{Al}_2\text{O}_3 - 0.326 \times \frac{\text{Fe}}{\text{Fe} + \text{Mg}} \quad 13.$$

while the compositional effect on the shear modulus and its pressure derivative of ferropericlase is given by:

$$G_0 = 127.8_{\text{HS}}/137_{\text{LS}} - 113.83 \times \frac{\text{Fe}}{\text{Fe} + \text{Mg}} \quad 14.$$

$$G' = 2.13_{\text{HS}}/2.08_{\text{LS}} - 1.182 \times \frac{\text{Fe}}{\text{Fe} + \text{Mg}} \quad 15.$$

where Al_2O_3 and $\text{Fe}/(\text{Fe}+\text{Mg})$ are given in terms of wt% and mole fraction, respectively, G_0 in GPa, and HS and LS refer to high- and low-spin state, respectively. V_P and V_S are subsequently obtained from the usual expressions:

$$V_P = \sqrt{\frac{K_S + \frac{4}{3}G}{\rho}} \quad \text{and} \quad V_S = \sqrt{\frac{G}{\rho}}, \quad 16.$$

where K_S and G are the adiabatic bulk and shear modulus at the desired lower mantle pressure and temperature. For the dependence of K_S on Al_2O_3 and $\text{Fe}/(\text{Fe}+\text{Mg})$, we followed Fu et al. (2023).

4.3. Combining mineral physics and geophysical constraints

To constrain the lower-mantle mineral assemblage and, in turn, composition, we construct lower-mantle mineral physics V_P , V_S , and density profiles relying on the assumption that the lower mantle is principally made up of the major minerals bridgmanite and ferropericlase, and attempt to find the mineral physics models for a range of bridgmanite/ferropericlase ratios, corresponding to volume fractions of 70%:30%, 80%:20%, 90%:10%, and 100%:0%, that provide the best fit to SC-REM. For the purpose of constructing lower-mantle seismic profiles based on the mineral physics data and EoSs compiled here, we rely on the lower-mantle geophysical adiabats (isentropes) of SC-REM (Kemper et al. 2023), which, as indicated in Figure 5a, is similar (within measurement, observational, and modeling uncertainties) to the laboratory-based peridotite geotherm of Katsura (2022).

Briefly, at the basis of SC-REM is a large set of normal-mode data that is much larger than what was available at the time of PREM, mantle and outer-core sensitive body waves, and the most up-to-date astronomic-geodetic measurements of mean mass and moment of inertia, including the degree-2 tidal response. As PREM has demonstrated, inversion of normal-mode centre frequencies represents a most efficient means to determining the average radial seismic structure of the Earth (Dziewonski and Anderson 1981).

To account for additional uncertainties associated with the mineral physics- and composition-related parameters that enter into the EoS (Eqs. 12–15), we conduct a Monte Carlo search of all relevant parameters. For each of the mineral configurations, we randomly vary the Al_2O_3 content in the range 3.8–4 wt% and Fe in bridgmanite and ferropericlase between 6–10 mol% and 20 and 22 mol%, respectively, while temperature varies between the upper and lower bounds of SC-REM shown in Figure 5a. The partition coefficient, K_D , of Fe between bridgmanite and ferropericlase, presently varies between 0.23 and 0.44, which is consistent with previous work (e.g., Murakami et al. 2005, Sinmyo et al. 2008, Irifune et al. 2010). The EoS parameters K_0 , K' , V_0 are varied within $\pm 0.5\%$, $\pm 0.75\%$, and $\pm 0.5\%$, respectively, relative to the values listed in Table 2. For the four constant-mineralogical models, this corresponds to variations in Mg/Si between 1.35–1.39 (bridgmanite/ferropericlase~70%:30%), 1.19–1.24 (bridgmanite/ferropericlase~80%:20%), 1.07–1.12 (bridgmanite/ferropericlase~90%:10%), and 1 (bridgmanite/ferropericlase~100%:0%), respectively. These parameter ranges provide a reasonable coverage of measurement uncertainties of various experimental groups (including Murakami et al. 2012, Mashino et al. 2020, Fu et al. 2023, Jackson and Rigden 1998). Aggregate V_P , V_S , and density profiles were computed using `Burnman` (Myhill et al. 2023) and are shown in Figure 5b–d as relative differences to the mean SC-REM model.

From our analysis and Figure 5, we can draw a number of conclusions. Firstly, the com-

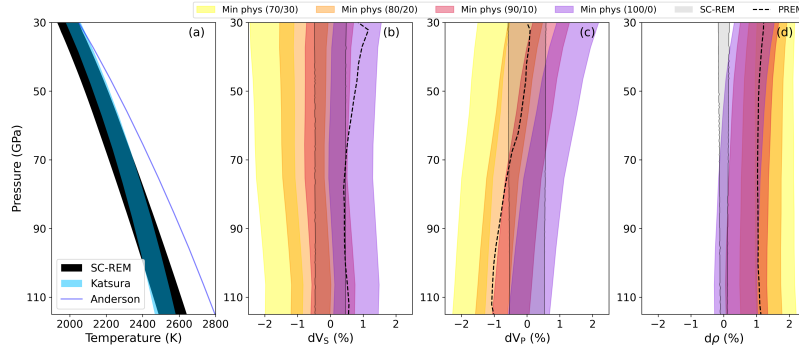


Figure 5

Comparison between experimentally-constrained mineral physics (MP) and geophysically-determined lower mantle seismic wave speed profiles. (A) Representative lower mantle geotherms: the laboratory-based peridotite adiabat (Katsura) (Katsura 2022), the geophysically-constrained isentropes (SC-REM) (Kemper et al. 2023), and a superadiabatic model geotherm (Anderson 1982). (B) Lower mantle MP and SC-REM S-wave speed (V_S) profiles; (C) P-wave (V_P) speed profiles; and (D) density (ρ) profiles. Panels B–D indicate relative differences computed as $dX = (dX_{MP} - d\hat{X}_{SC-REM}) / d\hat{X}_{SC-REM}$, where X is seismic property and $d\hat{X}_{SC-REM}$ and dX_{MP} are the equivalent properties in SC-REM (mean) and MP, respectively. The MP models in (B–D) are based on Monte Carlo modeling to account for measurement uncertainties in composition and mineral physics parameters and computed along the SC-REM geotherms for a lower mantle made up of a representative range of bridgmanite/ferropericlasite ratios (indicated by the numbers in parentheses in the legend). The range in SC-REM profiles shown here represents the 50% credible interval of the sampled model range. See main text for details.

bined variations in temperature, composition, and mineral physics parameters correspond to changes in V_S , V_P , and density of $\sim 1.3\%$, $\sim 1\%$, and $\sim 1.2\%$, respectively. Similar variations are obtained when changing the bridgmanite/ferropericlasite ratio by 10%. In comparison, uncertainties in V_S , V_P , and density in SC-REM are $\sim 0.8\%$, $\sim 1.2\%$, and $\sim 0.2\%$, respectively. Secondly, constant-compositional models with $Mg/Si \geq 1.2$ are generally too slow and too dense, while models with $Mg/Si \leq 1.2$ fare better, particularly as Mg/Si approaches 1. Thirdly, V_S can be matched by a constant-compositional lower mantle with a $Mg/Si \sim 1-1.12$, corresponding to a bridgmanite volume fraction of 90%–100%. In turn, the relative V_P profiles suggest a mineralogical, and therefore compositional, gradient with Mg/Si decreasing from $\sim 1.19-1.24$ in the 30–50 GPa pressure range over $1.07-1.12$ in the mid-to-lower mantle (50–80 GPa) to $1-1.12$ in the lowermost mantle (80–115 GPa), corresponding to an increasing bridgmanite fraction with depth. Finally, the mineral-physics models presented in Figure 5 yield higher densities than SC-REM, except for the pure bridgmanite model ($Mg/Si \sim 1$). Of our models, the latter model is also the only one capable of matching V_P , V_S , and density simultaneously across most of the lower mantle within uncertainty. Thus, we may summarise the comparison between geophysics and mineral physics as pointing to a cosmic lower mantle composition with a Mg/Si close to 1.

In interpreting the mineral physics profiles, however, a number of issues come into play that are of relevance for the present comparison. The mineral physics models are based on a “minimum” parameterisation that, while allowing for variations in lower-mineralogy (through changes in bridgmanite/ferropericlasite ratio), do not account for the thermally-

and compositionally-driven changes in bridgmanite/ferropericlasite ratio as a function of temperature, Al_2O_3 , and Fe, nor is the effect of the latter on Mg/Si fully captured. Also, adiabatic thermal conditions are implicit in our calculations. Although models with larger degrees of freedom (e.g., sub- and superadiabatic conditions, increase in the number of components in chemical model) are permissible, these only act to increase non-uniqueness, and were therefore not considered in the construction of SC-REM.

To study the impact of a superadiabatic lower mantle geothermal gradient, we considered the geotherm of Anderson (1982) (Figure 5a) and re-performed the Monte Carlo sampling of the mineral physics profiles as described above. The comparison (not shown) based on the thermal profile of Anderson (1982) indicates, as expected, a decrease in all modelled properties so as to produce changes in dV_S , dV_P , and $d\rho$ relative to the properties computed using SC-REM of about -0.75%, -0.3%, and -0.2%, respectively, exacerbating the match to the pure bridgmanite model. Since a superadiabatic lower mantle consisting purely of bridgmanite is unlikely to be realistic, this could possibly be an indicator for subadiabatic lower mantle conditions, consistent with geodynamic models (e.g., Yan et al. 2020). Finally, as illustrated in Figure 3, the mineral phase ca-pv is stable throughout the lower mantle at levels of ~ 5 vol%. To investigate the effect of ca-pv on mineral-physics profiles, we recomputed V_S , V_P , and density by allocating 5 vol% of bridgmanite/ferropericlasite to calcium-perovskite. The resultant changes in dV_S , dV_P , and $d\rho$ are around 0.2%, -0.1%, and 0.3%, respectively, and therefore insignificant.

5. The composition of Earth's lower mantle in the context of Earth evolution and dynamics

Numerical models of long-term mantle convection can be used integrate geochemical and geophysical data, placing them into the context of mantle structural evolution. However, the predictions of global-scale mantle-evolution models can strongly depend on the assumed initial condition, especially in terms of any compositional layering due to mantle differentiation (e.g., Kellogg et al. 1999, Davaille 1999). The initial thermo-chemical structure of the mantle is set in the aftermath of the Moon-forming giant impact, during which the entire mantle was likely molten as a global magma ocean (Nakajima and Stevenson 2015), but remains poorly understood.

5.1. Heterogeneity Formation in the Early Earth

Chemical fractionation during the crystallization of a deep magma ocean (MO) governs the initial composition of the mantle, crust and atmosphere. Initially, the hot MO cools quickly, and convects vigorously. As first crystals form, they either settle gravitationally (fractional crystallization), or remain in suspension (batch crystallization). In the latter case, a mush that behaves similar to a solid is formed at $\sim 40\%$ crystal fraction (Costa et al. 2009). The dominance of either mode of crystallization depends on the efficiency of crystal nucleation and growth, the liquid-solid density contrast, the viscosity of the silicate liquid, as well as the MO cooling history (Lebrun et al. 2013, Solomatov 2015). While fractional crystallization is likely dominant in the upper mantle (Solomatov 2015, Xie et al. 2020), the mode of lower-mantle MO crystallization remains poorly understood.

For any reasonable starting compositions of the whole-mantle MO (Mg/Si of 1.21~1.25 (Ringwood 1979, McDonough and Sun 1995, Palme and O'Neill 2014) or possibly lower),

Mg-rich Bridgmanite is the first phase to crystallize from the lower-mantle MO (Boukaré et al. 2015, Caracas et al. 2019, Nabeii et al. 2021). For efficient crystal setting (i.e., fractional crystallization), this implies a silica-enriched initial composition of the lower mantle with Mg/Si close to 1. For end-member batch crystallization (also referred to as “equilibrium crystallization” (Solomatov 2015)), the lower mantle would, in turn, assume a BSE composition in the aftermath of MO crystallization. However, end-member batch crystallization without any melt-solid segregation remains highly unlikely. Indeed, the crystal mush that is formed during batch crystallization cools very slowly. on the relevant timescales (of solid-state convection (Solomatov 2015)), melt-solid segregation due to coupled melt percolation and solid compaction should be efficient, possibly aided by convection (Holtzman et al. 2003, Hier-Majumder and Hirschmann 2017, Ballmer et al. 2017b, Caracas et al. 2019). As soon as the melt is extracted from the mush, the remaining solid is again a cumulate pile of bridgmanite with similar compositions as for fractional crystallization (Caracas et al. 2019). Thus, both end-member modes of MO crystallization lead to significant bridgmanite fractionation during Earth mantle differentiation, and possibly a silica-enriched lower mantle.

Alternative scenarios for the sequestration of silica-enriched heterogeneity in the early Earth involve incomplete equilibration of the mantle in the aftermath of a Moon-forming giant impact (Deng et al. 2019), as well as exsolution of SiO₂ from the core (Hirose et al. 2017, Helffrich et al. 2018). Assuming that significant amounts of silica have been partitioned into the core at the high-temperature conditions of the Moon-forming impact (Hirose et al. 2017), the flux of SiO₂ from the core to the mantle is $\sim 8 \times 10^{21}$ kg per 100 K of core cooling (Helffrich et al. 2018). For CMB temperatures ≥ 4750 , the thermally-coupled core-MO system is fully molten (Boukaré et al. 2015), such that any exsolved SiO₂ would be efficiently mixed across the BSE. For core temperatures of roughly 4750~4000 K, the mantle should be separated into two layers, i.e., a basal magma ocean (BMO) and the overlying MO/mantle (Boukaré et al. 2015, Caracas et al. 2019, Labrosse et al. 2007, Miyazaki and Korenaga 2019). Over this temperature range, the core can deliver up to $\sim 5.7 \times 10^{22}$ kg of SiO₂ (i.e., ~ 2 wt. % of the lower-mantle’s mass) to the BMO. After BMO freezing, the core continues to deliver SiO₂ to the lower mantle as small-scale blobs (Helffrich et al. 2018), but related amounts are small, as the BMO solidus (Boukaré et al. 2015, Miyazaki and Korenaga 2019) is close to the temperature of the present-day CMB (e.g., Anzellini et al. 2013, Nomura et al. 2014). Another process to deliver silica to the lowermost mantle, is the overturn of Hadean crust (Tolstikhin and Hofmann 2005), but this material may again interact with the BMO.

The crystallization of such a SiO₂-enriched BMO would have similar consequences for the fractionation of bridgmanitic cumulates as discussed above for the whole-mantle MO. For silica-normative (i.e., roughly molar (Mg+Fe)/Si ≤ 1.0) starting compositions, evolved BMO cumulates may involve some stishovite (SiO₂) (Boukaré et al. 2015). The total amount of fractionated bridgmanitic/stishovitic cumulates depends on the initial volume of the BMO (Caracas et al. 2019), as well as the influx of (Hadean) crust from above and core-exsolved SiO₂ from below.

5.2. Heterogeneity Preservation during Long-term Mantle Evolution

While it appears likely that silica-enriched materials are formed in the early-Earth, it remains uncertain whether such “primordial” heterogeneity can be preserved over time in

the solid-state convecting mantle. Seismic images of subducted slabs that sink through the mantle (e.g., Van Der Meer et al. 2010), as well as of mantle plumes that rise from the core-mantle boundary to the base of the lithosphere (French and Romanowicz 2015), support the notion that the mantle convects as a whole. Whole-mantle convection is highly efficient in mixing the mantle, particularly in the plate-tectonic regime (Ferrachat and Ricard 1998, O'Neill and Zhang 2018). At face value, this would imply that the lower mantle has essentially the same bulk composition as the pyrolitic uppermost mantle, and thus a relatively high Mg/Si ratio of ~ 1.26 . Considering lithospheric recycling over billions of years, most of the mantle is accordingly thought to be a small-scale mechanical mixture of recycled slab components, consistent with seismic observations (Morgan and Morgan 1999, Xu et al. 2008, Waszek et al. 2021, Goes et al. 2022) (also see section 3). A mechanical mixture of $\sim 20\%$ mafic/basaltic and $\sim 80\%$ harzburgitic rocks (i.e., with a “basalt fraction” $f=0.2$) approximates a pyrolitic composition with $\text{Mg/Si} \approx 1.27$, consistent with MORB source compositions (Ringwood 1975, 1979, Workman and Hart 2005, Xu et al. 2008) and volume estimates of past subduction (Morgan and Morgan 1999).

On the other hand, several geophysical observations are at odds with a mantle that is homogeneous on large scales with $f \approx 0.2$. For example, seismic profiles such as PREM and SC-REM cannot be matched with a uniform adiabatic mantle (see section 4.3 for details). In addition, some subducted slabs stagnate at $\sim 1,000$ km depth (Fukao and Obayashi 2013), which is difficult to reconcile with a well-stirred mantle, as this depth range is far from phase transformations (Figure 3). While a viscosity jump, which is also inferred at $\sim 1,000$ km depth from geoid inversion (Rudolph et al. 2015), may provide a viable explanation for slab stagnation, it does not readily account for the deflection of several plumes in a similar depth range (French and Romanowicz 2015), and more importantly, its occurrence by itself remains enigmatic. Intermediate-scale (1000s of km across) seismic reflectors/refractors in the uppermost lower mantle indicate regional compositional anomalies, possibly enriched in silica (Jenkins et al. 2017, Waszek et al. 2018). Thus, it cannot be ruled out that primordial heterogeneity (e.g., MO cumulates) is preserved in the lower mantle (Ballmer et al. 2017a).

Modelling studies have demonstrated that significant preservation is indeed geodynamically feasible as long as the primordial material is intrinsically viscous (Ballmer et al. 2017a, Gülcher et al. 2020, Gülcher et al. 2021). In these models, primordial material, initially imposed as a thick basal layer, can be preserved as small blobs to large domains in the mid-lower mantle (Figure 7), as up- and downwellings tend to flow around them to minimize viscous dissipation. These domains have been referred to as “bridgmanite-enriched ancient mantle structures” (BEAMS). They are thought to host bridgmanitic MO cumulates, but any primordial material would be preserved in a similar way, as long as their physical properties agree with those modelled. Over 4–5 billion years model time, preservation is most efficient (8%–30% of lower-mantle volume) for a viscosity of primordial material that is ≥ 2 orders of magnitude (and a density that is slightly) higher than the rest of the mantle. These physical properties are realistic for (slightly iron-enriched) bridgmanite (Tsujino et al. 2022), particularly when taking into consideration that the viscosity of ultramafic rocks should be controlled by that of ferropericlase (Girard et al. 2016), and that grain growth in bridgmanitic rocks is highly efficient (Fei et al. 2023). They are also consistent with primordial compositions that involve SiO_2 stishovite, which is even more viscous than bridgmanite (Xu et al. 2017).

Assuming that primordial materials are purely bridgmanitic, the implications in terms of BSE Mg/Si can be estimated. The sequestration of bridgmanitic material with a mass

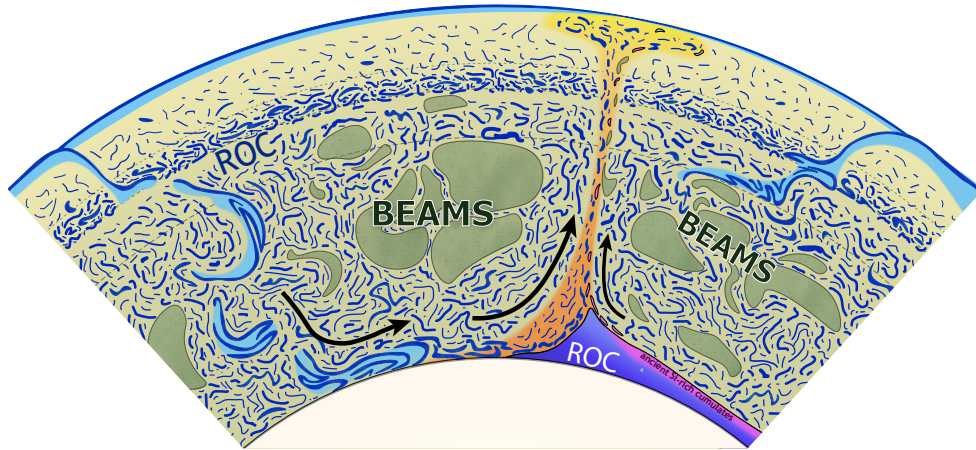


Figure 6

Visualization of a potential style of material preservation and present-day mantle structure, as based on geodynamic-model predictions (reproduced with modifications from Gülcher et al. (2021)). Recycled oceanic crust (ROC) is enriched in the transition zone and lower mantle. Bridgmanitic material may be preserved as BEAMS in the mid-mantle, e.g. explaining slab stagnation. Additional Si-enriched materials may be stored as piles in the lowermost mantle, and sampled by plumes (yellow). The depicted mantle structure is silica-enriched compared to a well-mixed mantle (e.g., mechanical mixture with $f=20\%$), but remains consistent with whole-mantle convection, and thus close to an end-member model in terms of silica enrichment (see section 5.3). Dashed lines mark depths of 410, 660 and 1000 km.

of $X_{bm} \leq 13\%$ of that of the mantle is within the range of that predicted by geodynamic models for BEAMS, and remains consistent with chondritic Ca/Sc and Ca/Yb (Liebske et al. 2005) (see also section 2). Assuming that this material is buried in the lower mantle, and independent of its geometry (e.g., as BEAMS, small blobs, or otherwise), it would shift the BSE Mg/Si ratio from ~ 1.27 (i.e., convecting mantle with $f=0.2$, see above) to ≥ 1.22 .

Even though BEAMS potentially provide an attractive reservoir for excess silica in the lower mantle, to date, there is no unequivocal evidence for their actual presence and long-term preservation. Models predict the roofs of BEAMS to be typically located at 800~1,200 km depth (Gülcher et al. 2020, Gülcher et al. 2021), consistent with the depths of regional seismic reflectors/refractors, the inferred viscosity jump and stagnant slabs. On the other hand, the BEAMS model is difficult to test by seismic tomography, as bridgmanite is only slightly faster than a pyrolytic bridgmanite-ferropericlasite assemblage (80/20 in Fig. 5). Moreover, geodynamic models predict that BEAMS are also slightly warmer than the ambient mantle (Gülcher et al. 2021), hence trading off with their slightly higher intrinsic thermoelastic properties. That being said, comparison of the footprints of relatively fast vs. slow S- and P-velocity regions in the mid-lower mantle are consistent with BEAMS (Shephard et al. 2021). Additional studies are needed to further test the BEAMS hypothesis, particularly exploiting seismic attenuation and anisotropy, or even magnetotellurics, but at present, all these methods have a limited resolution in the lower mantle.

5.3. Enrichment of basaltic rocks in the convecting lower mantle

In contrast to BEAMS, which evolve from an intrinsically strong layer of MO cumulates, an alternative scenario for silica sequestration in the lower mantle is independent of the initial condition of mantle convection. Significant amounts of basaltic rocks have been recycled into the mantle over billions of years (Morgan and Morgan 1999). Even before the onset of plate tectonics, crustal recycling has likely been efficient during alternative regimes of global tectonics (Sizova et al. 2010, Moore and Webb 2013, Lourenço et al. 2020). Basaltic rocks are denser than ultramafic rocks (e.g., pyrolite, harzburgite) across most of the mantle, except for a narrow depth range between 660 km and 700~750 km depth. Due to this density crossover, geodynamic models predict that the mantle transition zone acts as a “basalt filter”, such that small-scale basaltic heterogeneity tends to be enhanced in the transition zone as well as the lower mantle relative to the upper mantle (Nakagawa and Buffett 2005, Ballmer et al. 2015, Yan et al. 2020). These model predictions are well supported by seismic precursor studies, which provide evidence for a heterogeneous and basalt-enriched transition zone (Tauzin et al. 2022, Bissig et al. 2022b, Goes et al. 2022).

A picture emerges, in which the convecting mantle is still a mechanical mixture of mafic (ancient and modern recycled basalt) and ultramafic (harzburgite and peridotite/pyrolite) rocks, but with variable proportions (i.e., variable f) across the mantle. According to Yan et al. (2020), an average $f \approx 0.25$ in the convecting mantle corresponds to a pyroclitic uppermost mantle (i.e., $f \approx 0.2$), balanced by higher f in the transition zone and lower mantle. This model is overall consistent with seismic constraints for $f \approx 0.2$ – 0.5 in the transition zone (Munch et al. 2020, Bissig et al. 2022a,b, Tauzin et al. 2022), and implies Mg/Si ≈ 1.2 for the BSE, in accord with primitive-mantle estimates of Mg/Si ≈ 1.21 (see section 2). A more precise estimate is not just limited by model limitations and choices in Yan et al. (2020), but moreover requires assumptions on how much of the basaltic material that floats in the lower mantle (or is piled up at its base (Brandenburg and Van Keken 2007)) is modern MORB, and how much of it is ancient basaltic material. Ancient basalts with ages ≥ 2 Ga display significantly higher Mg/Si and Ca/Al than modern MORB (Herzberg et al. 2010), and thus tend to shift inferred BSE values as long as they are preserved in significant fractions. Indeed, significant preservation of ancient recycled crust in the lower mantle is consistent with geodynamic modelling (Yan et al. 2020) and isotope geochemical data (Cabral et al. 2013).

5.4. Implications for BSE composition

Figure 7 summarizes the coupled effects of ancient basalt and bridgmanite preservation, as well as those of total basalt fraction (f) in the convecting mantle, on BSE Mg/Si (contours) and Ca/Al (colors). Neglecting the basalt filter (i.e., $f \approx 0.2$), BSE Mg/Si are generally high, even for significant bridgmanite preservation. The minimum permitted Mg/Si is ~ 1.24 as long as significant fractions of basaltic material stored in the mantle are ancient (≥ 2 Ga), a condition to match chondritic Ca/Al of 0.72~0.74 (McDonough and Sun 1995, Palme and O’Neill 2014). Taking into account the basalt filter (i.e., $f \approx 0.25$), BSE Mg/Si can be significantly lower, i.e. well within the range of primitive-mantle compositions (Palme and O’Neill 2014). Combining the effects of the basalt filter with those of bridgmanite preservation ($X_{bm} \leq 0.13$, e.g., due to BEAMS) yields BSE Mg/Si ~ 1.18 , and further combining with those of ancient-basalt preservation, ~ 1.16 . These BSE Mg/Si correspond to lower-mantle Mg/Si of 1.14~1.16.

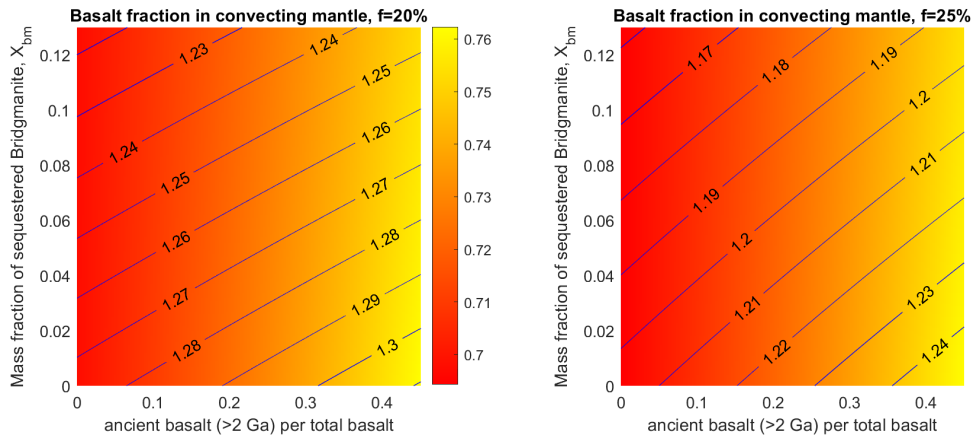


Figure 7

BSE composition (contours: molar Mg/Si, colors: molar Ca/Al) for a mantle that consists of preserved bridgmanite with fractions of X_{bm} within a basalt-harzburgite mechanical mixture. In this mechanical mixture, basalt fractions are (left) $f=20\%$ and (right) $f=25\%$. The basaltic component within this mixture is partly modern MORB, and partly ancient basalt with ages ≥ 2 Ga as labelled (x-axis). Bridgmanite (magma-ocean cumulates), harzburgite, modern MORB and ancient basalt compositions are taken from Caracas et al. (2019), Baker and Beckett (1999), Workman and Hart (2005) and Herzberg et al. (2010), respectively.

It should be noted that these values are likely lower bounds. Lower-mantle bridgmanite preservation may be less efficient than assumed above, depending on the viscosity and density of the bridgmanitic layer formed during Earth differentiation (Gülcher et al. 2020, Gülcher et al. 2021). On the other hand, exsolution of SiO_2 from the core (Hirose et al. 2017, Helffrich et al. 2018) can further reduce lower-mantle Mg/Si, but just by ≤ 0.02 relative. This limited effect is because exsolution primarily occurs during the lifetime of the BMO (see 5.1), and is thus already included in the budget of bridgmanitic cumulates above, unless BMO cumulates include significant fractions of stishovite (see 5.1) and are preserved in the lower mantle, a model that has testable geophysical implications (Yang and Wu 2014). Independent of their origin, the large-low velocity provinces are another potentially silica-enriched reservoir (Trampert et al. 2004, Vilella et al. 2021). However, as long as they are made up of basalt (or materials with similar Mg/Si), their effects are already included in the budget discussed above (Figure 7).

6. Summary

If the mantle has been recycled and stirred efficiently due to plate subduction for at least 2–3 Gyrs (Korenaga 2013), a BSE Mg/Si ratio significantly lower than 1.15–1.18 seems unlikely based on geodynamical considerations (section 5). However, there still remains significant debate over changes in mantle convection patterns throughout Earth’s history. The compilation of geochemical studies indicates a lower-mantle Mg/Si of 1.12–1.16. (section 2.4). For a simplified bi-mineralic model, these Mg/Si values translate to a bridgmanite-to-ferropericline volume ratio of $\sim 85:15$. The mineral physics approach, which involves comparing experimentally-determined shear wave velocity data with 1-D seismological model, overall points to a cosmic lower mantle composition with a Mg/Si ratio close to 1 ($\sim 100\%$

bridgmanite). However, the assumed lower mantle mineral assemblage of bridgmanite and ferropericlase may be too simplistic to account for the potential mismatch between the experimental data and seismic model. To comprehensively explain the apparent mismatch with radial seismic reference models, it may be necessary to consider radial variations in bulk composition, and notably, small-to-medium scale lateral heterogeneity. The mantle is heterogeneous on a wide range of scales (e.g., recycled materials, primordial heterogeneity), and this macro-scale heterogeneity should be accounted for during the inversion of geophysical data.

FUTURE ISSUES

1. A better understanding of 1) the bulk composition of the Earth relative to the chondritic paradigm for major elements, particularly Fe, Mg and Si, and 2) the Si content of the core is needed to break the degeneracy between plausible compositional models of the lower mantle.
2. Additional high P-T experiments with varying iron content are required for improved understanding of the effects of the Fe-spin transition on the elasticity of bridgmanite and ferropericlase.
3. Further need of evaluation of the effect of the coupled incorporation of Fe³⁺ and Al₂O₃ on bridgmanite elasticity.
4. A more definitive approach to comparing mineral physics measurements with geophysical data/models would be to merge the experimental data with the thermodynamic database for the relevant end-members and re-perform the geophysical inversion following the approach laid out here. This would ensure that the derived models of interior structure are based on 1) geophysical data, including full consideration of data uncertainties; 2) quantitative comparison with data; 3) a variable compositional and mineralogical model, including the most up-to-date thermoelastic parameters; 4) self-consistent model computations; and, finally, 5) encapsulating uncertainties in thermodynamic parameters either *a posteriori* via a hybrid strategy or directly in the inversion.
5. To better understand the dynamics of mixing and preservation of silica-enriched heterogeneity in the (lower) mantle, numerical models with more realistic rheology (e.g., grain-size and fabric dependent) and distribution of heat-producing elements are needed.
6. Future geodynamic models should also aim to treat the transition from magma-ocean crystallization to solid-state convection and long-term mantle evolution self-consistently.

Acknowledgements

The authors are grateful to Federico D. Munch for help with Figures 3 and 5. We also thank Roberta Rudnick for comments on the paper.

LITERATURE CITED

G. A. Abers and B. R. Hacker. A MATLAB toolbox and Excel workbook for calculating the densities, seismic wave speeds, and major element composition of minerals and rocks at pressure

- and temperature. *Geochemistry, Geophysics, Geosystems*, 17(2):616–624, Feb. 2016. .
- J. C. Afonso, J. Fullea, W. L. Griffin, Y. Yang, A. G. Jones, J. A. D. Connolly, and S. Y. O’Reilly. 3-D multiobservable probabilistic inversion for the compositional and thermal structure of the lithosphere and upper mantle. I: a priori petrological information and geophysical observables. *Journal of Geophysical Research (Solid Earth)*, 118(5):2586–2617, May 2013. .
- C. J. Allègre, J.-P. Poirier, E. Humler, and A. W. Hofmann. The chemical composition of the Earth. *Earth and Planetary Science Letters*, 134(3):515–526, Sept. 1995. .
- O. L. Anderson. The earth’s core and the phase-diagram of iron. *Phil. Trans. R. Soc. Lond. A*, 306:21–35, 1982. .
- S. Anzellini, A. Dewaele, M. Mezouar, P. Loubeyre, and G. Morard. Melting of iron at earth’s inner core boundary based on fast x-ray diffraction. *Science*, 340(6131):464–466, 2013.
- J. Badro. Spin transitions in mantle minerals. *Annu. Rev. Earth Planet. Sci.*, 42, 2014a. .
- J. Badro. Spin transitions in mantle minerals. *Annual Review of Earth and Planetary Sciences*, 42:231–248, 2014b.
- J. Badro, A. S. Côté, and J. P. Brodholt. A seismologically consistent compositional model of earth’s core. *Proceedings of the National Academy of Sciences*, 111(21):7542–7545, 2014.
- M. B. Baker and J. R. Beckett. The origin of abyssal peridotites: a reinterpretation of constraints based on primary bulk compositions. *Earth and Planetary Science Letters*, 171(1):49–61, 1999.
- M. B. Baker and E. M. Stolper. Determining the composition of high-pressure mantle melts using diamond aggregates. *Geochimica et Cosmochimica Acta*, 58(13):2811–2827, 1994.
- M. D. Ballmer, N. C. Schmerr, T. Nakagawa, and J. Ritsema. Compositional mantle layering revealed by slab stagnation at ~ 1000-km depth. *Science advances*, 1(11):e1500815, 2015.
- M. D. Ballmer, C. Houser, J. W. Hernlund, R. M. Wentzcovitch, and K. Hirose. Persistence of strong silica-enriched domains in the earth’s lower mantle. *Nature Geoscience*, 10(3):236–240, 2017a.
- M. D. Ballmer, D. L. Lourenço, K. Hirose, R. Caracas, and R. Nomura. Reconciling magma-ocean crystallization models with the present-day structure of the earth’s mantle. *Geochemistry, Geophysics, Geosystems*, 18(7):2785–2806, 2017b.
- C. Bina and G. Helffrich. 3.2 - geophysical constraints on mantle composition. In H. D. Holland and K. K. Turekian, editors, *Treatise on Geochemistry (Second Edition)*, pages 41–65. Elsevier, Oxford, second edition edition, 2014. ISBN 978-0-08-098300-4. .
- C. R. Bina. Free Energy Minimization by Simulated Annealing with Applications to Lithospheric Slabs and Mantle Plumes. *Pure and Applied Geophysics*, 151(2-4):605–618, Jan. 1998. .
- F. Bissig, A. Khan, and D. Giardini. Evidence for basalt enrichment in the mantle transition zone from inversion of triplicated P- and S-waveforms. *Earth and Planetary Science Letters*, 580:117387, 2022a.
- F. Bissig, A. Khan, and D. Giardini. Joint inversion of PP and SS precursor waveforms and rayleigh wave phase velocities for global mantle transition zone structure. *Geophysical Journal International*, pages 1–24, 2022b. .
- C.-E. Boukaré, Y. Ricard, and G. Fiquet. Thermodynamics of the mgo-feo-sio2 system up to 140 gpa: Application to the crystallization of earth’s magma ocean. *Journal of Geophysical Research: Solid Earth*, 120(9):6085–6101, 2015.
- F. Boyd. Compositional distinction between oceanic and cratonic lithosphere. *Earth and Planetary Science Letters*, 96(1-2):15–26, 1989.
- J. Brandenburg and P. Van Keken. Deep storage of oceanic crust in a vigorously convecting mantle. *Journal of Geophysical Research: Solid Earth*, 112(B6), 2007.
- R. A. Cabral, M. G. Jackson, E. F. Rose-Koga, K. T. Koga, M. J. Whitehouse, M. A. Antonelli, J. Farquhar, J. M. Day, and E. H. Hauri. Anomalous sulphur isotopes in plume lavas reveal deep mantle storage of archaean crust. *Nature*, 496(7446):490–493, 2013.
- F. Cammarano, S. Goes, A. Deuss, and D. Giardini. Is a pyrolitic adiabatic mantle compatible with seismic data? *Earth and Planetary Science Letters*, 232(3-4):227–243, Apr. 2005. .

- D. Canil. Mildly incompatible elements in peridotites and the origins of mantle lithosphere. *Lithos*, 77(1-4):375–393, 2004.
- R. Caracas, K. Hirose, R. Nomura, and M. D. Ballmer. Melt–crystal density crossover in a deep magma ocean. *Earth and Planetary Science Letters*, 516:202–211, 2019.
- T. C. Chust, G. Steinle-Neumann, D. Dolejš, B. S. A. Schuberth, and H. P. Bunge. MMA-EoS: A Computational Framework for Mineralogical Thermodynamics. *Journal of Geophysical Research (Solid Earth)*, 122(12):9881–9920, Dec. 2017. .
- L. Cobden, S. Goes, M. Ravenna, E. Styles, F. Cammarano, K. Gallagher, and J. A. D. Connolly. Thermochemical interpretation of 1-D seismic data for the lower mantle: The significance of nonadiabatic thermal gradients and compositional heterogeneity. *Journal of Geophysical Research (Solid Earth)*, 114(B11):B11309, Nov. 2009. .
- J. A. D. Connolly. The geodynamic equation of state: What and how. *Geochem. Geophys. Geosyst.*, 10(10):1–19, 2009. .
- J. A. D. Connolly and D. M. Kerrick. Metamorphic controls on seismic velocity of subducted oceanic crust at 100–250 km depth. *Earth and Planetary Science Letters*, 204(1-2):61–74, Nov. 2002. .
- J. A. D. Connolly and A. Khan. Uncertainty of mantle geophysical properties computed from phase equilibrium models. *Geophys. Res. Lett.*, 43:1–9, 2016. .
- A. Corgne, C. Liebske, B. J. Wood, D. C. Rubie, and D. J. Frost. Silicate perovskite–melt partitioning of trace elements and geochemical signature of a deep perovskitic reservoir. *Geochimica et Cosmochimica Acta*, 69(2):485–496, 2005.
- A. Costa, L. Caricchi, and N. Bagdassarov. A model for the rheology of particle-bearing suspensions and partially molten rocks. *Geochemistry, Geophysics, Geosystems*, 10(3), 2009.
- G. Criniti, A. Kurnosov, T. Boffa Ballaran, and D. J. Frost. Single-crystal elasticity of $mgsio_3$ bridgmanite to mid-lower mantle pressure. *Journal of Geophysical Research: Solid Earth*, 126, 2021. .
- C. R. S. da Silva, R. M. Wentzcovitch, A. Patel, G. D. Price, and S. I. Karato. The composition and geotherm of the lower mantle: constraints from the elasticity of silicate perovskite. *Physics of the Earth and Planetary Interiors*, 118(1-2):103–109, Feb. 2000. .
- N. Dauphas, F. Poitrasson, C. Burkhardt, H. Kobayashi, and K. Kurosawa. Planetary and meteoritic mg/si and $\delta^{30}Si$ variations inherited from solar nebula chemistry. *Earth and Planetary Science Letters*, 427:236–248, 2015.
- A. Davaille. Simultaneous generation of hotspots and superswells by convection in a heterogeneous planetary mantle. *Nature*, 402(6763):756–760, 1999.
- H. Deng, M. D. Ballmer, C. Reinhardt, M. M. Meier, L. Mayer, J. Stadel, and F. Benitez. Primordial earth mantle heterogeneity caused by the moon-forming giant impact? *The Astrophysical Journal*, 887(2):211, 2019.
- S. M. Dorfman and T. S. Duffy. Effect of fe-enrichment on seismic properties of perovskite and post-perovskite in the deep lower mantle. *Geophysical Journal International*, 197:910–919, 2014. .
- A. M. Dziewonski and D. L. Anderson. Preliminary reference earth model. *Phys. Earth Planet. Inter.*, 25:297–356, 1981. .
- O. Fabrichnaya, K. Saxena, P. Richet, and E. F. Westrum. In *Thermodynamic Data, Models, and Phase Diagrams in Multicomponent Oxide Systems*. Springer, Heidelberg, 2004. .
- H. Fei, M. D. Ballmer, U. Faul, N. Walte, W. Cao, and T. Katsura. Variation in bridgmanite grain size accounts for the mid-mantle viscosity jump. *Nature*, pages 1–6, 2023.
- Y. Fei, L. Zhang, A. Corgne, H. Watson, A. Ricolleau, Y. Meng, and V. Prakapenka. Spin transition and equations of state of (mg, fe)o solid solutions. *Geophys. Res. Lett.*, 34:L17307, 2007. .
- S. Ferrachat and Y. Ricard. Regular vs. chaotic mantle mixing. *Earth and Planetary Science Letters*, 155(1-2):75–86, 1998.
- C. Fitoussi, B. Bourdon, T. Kleine, F. Oberli, and B. C. Reynolds. Si isotope systematics of meteorites and terrestrial peridotites: implications for mg/si fractionation in the solar nebula

- and for si in the earth's core. *Earth and Planetary Science Letters*, 287(1-2):77–85, 2009.
- S. W. French and B. Romanowicz. Broad plumes rooted at the base of the earth's mantle beneath major hotspots. *Nature*, 525(7567):95–99, 2015.
- P. Frossard, C. Israel, A. Bouvier, and M. Boyet. Earth's composition was modified by collisional erosion. *Science*, 377(6614):1529–1532, 2022.
- D. J. Frost and R. Myhill. Chemistry of the lower mantle. *Deep Earth: Physics and Chemistry of the Lower Mantle and Core*, pages 225–240, 2016.
- S. Fu, Y. Zhang, T. Okuchi, and J. F. Lin. Single-crystal elasticity of (al,fe)-bearing bridgmanite up to 82 gpa. *Am. Miner.*, 108:719–730, 2023. .
- Y. Fukao and M. Obayashi. Subducted slabs stagnant above, penetrating through, and trapped below the 660 km discontinuity. *Journal of Geophysical Research: Solid Earth*, 118(11):5920–5938, 2013.
- J. Fullea, S. Lebedev, Z. Martinec, and N. L. Celli. WINTERC-G: mapping the upper mantle thermochemical heterogeneity from coupled geophysical–petrological inversion of seismic waveforms, heat flow, surface elevation and gravity satellite data. *Geophys. J. Int.*, 226:146–191, 2021. .
- J. Ganguly, A. M. Freed, and S. K. Saxena. Density profiles of oceanic slabs and surrounding mantle: Integrated thermodynamic and thermal modeling, and implications for the fate of slabs at the 660 km discontinuity. *Physics of the Earth and Planetary Interiors*, 172(3-4):257–267, Feb. 2009. .
- J. Girard, G. Amulele, R. Farla, A. Mohiuddin, and S.-i. Karato. Shear deformation of bridgmanite and magnesiowüstite aggregates at lower mantle conditions. *Science*, 351(6269):144–147, 2016.
- S. Goes, C. Yu, M. D. Ballmer, J. Yan, and R. D. van der Hilst. Compositional heterogeneity in the mantle transition zone. *Nature Reviews Earth & Environment*, 3(8):533–550, 2022.
- A. V. Grayver, F. D. Munch, A. V. Kuvshinov, A. Khan, T. J. Sabaka, and L. Tøffner-Clausen. Joint inversion of satellite-detected tidal and magnetospheric signals constrains electrical conductivity and water content of the upper mantle and transition zone. *Geophysical research letters*, 44(12):6074–6081, 2017.
- A. J. Gülcher, D. J. Gebhardt, M. D. Ballmer, and P. J. Tackley. Variable dynamic styles of primordial heterogeneity preservation in the earth's lower mantle. *Earth and Planetary Science Letters*, 536:116160, 2020.
- A. J. P. Gülcher, M. D. Ballmer, and P. J. Tackley. Coupled dynamics and evolution of primordial and recycled heterogeneity in earth's lower mantle. *Solid Earth*, 12(9):2087–2107, 2021.
- B. R. Hacker and G. A. Abers. Subduction Factory 3: An Excel worksheet and macro for calculating the densities, seismic wave speeds, and H₂O contents of minerals and rocks at pressure and temperature. *Geochemistry, Geophysics, Geosystems*, 5(1):Q01005, Jan. 2004. .
- S. R. Hart and A. Zindler. In search of a bulk Earth composition. *Chemical Geology*, 57:247–267, Jan. 1986. .
- G. Helffrich, M. D. Ballmer, and K. Hirose. Core-exsolved sio₂ dispersal in the earth's mantle. *Journal of Geophysical Research: Solid Earth*, 123(1):176–188, 2018.
- C. Herzberg. Geodynamic information in peridotite petrology. *Journal of Petrology*, 45(12):2507–2530, 2004.
- C. Herzberg and P. Asimow. Primelt 3 mega. xlsx software for primary magma calculation: peridotite primary magma mgo contents from the liquidus to the solidus. *Geochemistry, Geophysics, Geosystems*, 16(2):563–578, 2015.
- C. Herzberg, K. Condie, and J. Korenaga. Thermal history of the earth and its petrological expression. *Earth and Planetary Science Letters*, 292(1-2):79–88, 2010.
- S. Hier-Majumder and M. M. Hirschmann. The origin of volatiles in the earth's mantle. *Geochemistry, Geophysics, Geosystems*, 18(8):3078–3092, 2017.
- K. Hirose, G. Morard, R. Sinmyo, K. Umemoto, J. Hernlund, G. Helffrich, and S. Labrosse. Crystallization of silicon dioxide and compositional evolution of the earth's core. *Nature*, 543(7643):99–102, 2017.

- K. Hirose, B. Wood, and L. Vočadlo. Light elements in the earth's core. *Nature Reviews Earth & Environment*, 2(9):645–658, 2021.
- B. Holtzman, N. Groebner, M. Zimmerman, S. Ginsberg, and D. Kohlstedt. Stress-driven melt segregation in partially molten rocks. *Geochemistry, Geophysics, Geosystems*, 4(5), 2003.
- D. Huang, J. Badro, J. Brodholt, and Y. Li. Ab initio molecular dynamics investigation of molten Fe–Si–O in earth's core. *Geophysical Research Letters*, 46(12):6397–6405, 2019.
- R. Huang, T. B. Ballaran, C. A. McCammon, N. Miyajima, D. Dolejš, and D. J. Frost. The composition and redox state of bridgmanite in the lower mantle as a function of oxygen fugacity. *Geochimica et Cosmochimica Acta*, 303:110–136, 2021.
- T. Irifune. Phase Transformations in Pyrolite and Subducted Crust Compositions down to a Depth of 800 km in the Lower Mantle. *Mineralogical Magazine*, 58A(1):444–445, Jan. 1994. .
- T. Irifune, T. Shimpei, C. McCammon, N. Miyajima, D. Rubie, and D. Frost. Iron partitioning and density changes of pyrolite in earth's lower mantle. *Science*, 327:193–195, 2010. .
- J. Ita and L. Stixrude. Petrology, elasticity, and composition of the mantle transition zone. , 97 (B5):6849–6866, May 1992. .
- C. R. Jackson, L. B. Ziegler, H. Zhang, M. G. Jackson, and D. R. Stegman. A geochemical evaluation of potential magma ocean dynamics using a parameterized model for perovskite crystallization. *Earth and Planetary Science Letters*, 392:154–165, 2014.
- I. Jackson. Elasticity, composition and temperature of the Earth's lower mantle: a reappraisal. *Geophysical Journal International*, 134(1):291–311, July 1998. .
- I. Jackson and S. M. Rigden. Composition and temperature of the earth's mantle: Seismological models interpreted through experimental studies of earth materials. *The Earth's Mantle: Composition, Structure and Evolution*, pages 405–460, 1998.
- J. M. Jackson, J. Zhang, J. Shu, S. V. Sinogeikin, and J. D. Bass. High-pressure sound velocities and elasticity of aluminous $MgSiO_3$ perovskite to 45 gpa: Implications for lateral heterogeneity in earth's lower mantle. *Geophys. Res. Lett.*, 32:L21305, 2005. .
- E. Jagoutz, H. Palme, H. Baddenhausen, K. Blum, M. Cendales, G. Dreibus, B. Spettel, V. Lorenz, and H. Wänke. The abundances of major, minor and trace elements in the earth's mantle as derived from primitive ultramafic nodules. In *In: Lunar and Planetary Science Conference, 10th, Houston, Tex., March 19-23, 1979, Proceedings. Volume 2. (A80-23617 08-91) New York, Pergamon Press, Inc., 1979, p. 2031-2050. Research supported by the Deutsche Forschungsgemeinschaft.*, volume 10, pages 2031–2050, 1979.
- J. Jenkins, A. Deuss, and S. Cottaar. Converted phases from sharp 1000 km depth mid-mantle heterogeneity beneath western Europe. *Earth and Planetary Science Letters*, 459:196–207, 2017.
- F. E. Jenner and H. S. C. O'Neill. Analysis of 60 elements in 616 ocean floor basaltic glasses. *Geochemistry, Geophysics, Geosystems*, 13(2), 2012.
- S. Kaneshima and G. Helffrich. Small scale heterogeneity in the mid-lower mantle beneath the circum-pacific area. *Physics of the Earth and Planetary Interiors*, 183(1-2):91–103, 2010.
- T. Katsura. A revised adiabatic temperature profile for the mantle. *Journal of Geophysical Research: Solid Earth*, 127(2):e2021JB023562, 2022. . e2021JB023562 2021JB023562.
- L. H. Kellogg, B. H. Hager, and R. D. van der Hilst. Compositional stratification in the deep mantle. *Science*, 283(5409):1881–1884, 1999.
- J. Kemper, A. Khan, G. Helffrich, M. van Driel, and D. Giardini. Self-consistent models of Earth's mantle and core from long-period seismic and tidal constraints. *Geophysical Journal International*, page gead254, 06 2023. ISSN 0956-540X. .
- B. L. N. Kennett and I. Jackson. Optimal equations of state for mantle minerals from simultaneous non-linear inversion of multiple datasets. *Physics of the Earth and Planetary Interiors*, 176(1-2): 98–108, Sept. 2009. .
- A. Khan. On Earth's Mantle Constitution and Structure from Joint Analysis of Geophysical and Laboratory-Based Data: An Example. *Surveys in Geophysics*, 37:1–21, 2016. .
- A. Khan, J. A. D. Connolly, and N. Olsen. Constraining the composition and thermal state of the

- mantle beneath Europe from inversion of long-period electromagnetic sounding data. *Journal of Geophysical Research (Solid Earth)*, 111(B10):B10102, Oct. 2006. .
- A. Khan, J. A. D. Connolly, and S. R. Taylor. Inversion of seismic and geodetic data for the major element chemistry and temperature of the earth’s mantle. *Journal of Geophysical Research: Solid Earth*, 113(B9), 2008. .
- A. Khan, L. Boschi, and J. A. D. Connolly. On mantle chemical and thermal heterogeneities and anisotropy as mapped by inversion of global surface wave data. *J. Geophys. Res.*, 114(B09305): 1–21, 2009. .
- A. Khan, P. A. Sossi, C. Liebske, A. Rivoldini, and D. Giardini. Geophysical and cosmochemical evidence for a volatile-rich mars. *Earth and Planetary Science Letters*, 578:117330, 2022.
- J. Korenaga. Initiation and evolution of plate tectonics on earth: theories and observations. *Annual review of earth and planetary sciences*, 41:117–151, 2013.
- T. Koyama, A. Khan, and A. Kuvshinov. Three-dimensional electrical conductivity structure beneath Australia from inversion of geomagnetic observatory data: evidence for lateral variations in transition-zone temperature, water content and melt. *Geophysical Journal International*, 196(3):1330–1350, Mar. 2014. .
- A. Kurnosov, H. Marquardt, D. J. Frost, T. B. Ballaran, and L. Ziberna. Evidence for a fe^{3+} -rich pyrolytic lower mantle from (al,fe)-bearing bridgmanite elasticity data. *Nature*, 543:543–546, 2017. .
- O. L. Kuskov and O. B. Fabrichnaya. Constitution of the Moon: 2. Composition and seismic properties of the lower mantle. *Physics of the Earth and Planetary Interiors*, 83(3-4):197–216, June 1994. .
- S. Labrosse, J. Hernlund, and N. Coltice. A crystallizing dense magma ocean at the base of the earth’s mantle. *Nature*, 450(7171):866–869, 2007.
- J. W. Larimer. Chemical fractionations in meteorites—i. condensation of the elements. *Geochimica et Cosmochimica Acta*, 31(8):1215–1238, 1967.
- H. C. Lau, J. X. Mitrovica, J. Austermann, O. Crawford, D. Al-Attar, and K. Latychev. Inferences of mantle viscosity based on ice age data sets: Radial structure. 121(10):6991–7012, 2016.
- H. C. Lau, J. X. Mitrovica, J. L. Davis, J. Tromp, H.-Y. Yang, and D. Al-Attar. Tidal tomography constrains Earth’s deep-mantle buoyancy. *Nature*, 551(7680):321, 2017.
- T. Lebrun, H. Massol, E. Chassefière, A. Davaille, E. Marcq, P. Sarda, F. Leblanc, and G. Brandeis. Thermal evolution of an early magma ocean in interaction with the atmosphere. *Journal of Geophysical Research: Planets*, 118(6):1155–1176, 2013.
- C. Liebske, A. Corgne, D. J. Frost, D. C. Rubie, and B. J. Wood. Compositional effects on element partitioning between mg-silicate perovskite and silicate melts. *Contributions to Mineralogy and Petrology*, 149:113–128, 2005.
- J. F. Lin, Z. Mao, J. Yang, and S. Fu. Elasticity of lower-mantle bridgmanite. *Nature*, 564:E18–E26, 2018. .
- K. Lodders. Solar system abundances and condensation temperatures of the elements. *The Astrophysical Journal*, 591(2):1220, 2003.
- D. L. Lourenço, A. B. Rozel, M. D. Ballmer, and P. J. Tackley. Plutonic-squishy lid: a new global tectonic regime generated by intrusive magmatism on earth-like planets. *Geochemistry, Geophysics, Geosystems*, 21(4):e2019GC008756, 2020.
- S. Lundin, K. Catalli, J. Santillán, S. H. Shim, V. B. Prakapenka, M. Kunz, and Y. Meng. Effect of fe on the equation of state of mantle silicate perovskite over 1mbar. *Phys. Earth Planet. Inter.*, 168:97–102, 2008. .
- T. Lyubetskaya and J. Korenaga. Chemical composition of Earth’s primitive mantle and its variance: 1. Method and results. *Journal of Geophysical Research (Solid Earth)*, 112(B3):B03211, Mar. 2007. .
- M. Manga. Mixing of heterogeneities in the mantle: Effect of viscosity differences, 1996. ISSN 00948276.

- I. Mashino, M. Murakami, N. Miyajima, and S. Petitgirard. Experimental evidence for silica-enriched earth's lower mantle with ferrous iron dominant bridgmanite. *Proceedings of the National Academy of Sciences*, 117:27899–27905, 2020. .
- J. Matas, J. Bass, Y. Ricard, E. Mattern, and M. S. T. Bukowinski. On the bulk composition of the lower mantle: predictions and limitations from generalized inversion of radial seismic profiles. *Geophysical Journal International*, 170(2):764–780, Aug. 2007. .
- K. J. Matthews, K. T. Maloney, S. Zahirovic, S. E. Williams, M. Seton, and R. D. Müller. Global plate boundary evolution and kinematics since the late paleozoic. *Global and Planetary Change*, 146:226–250, 2016.
- W. F. McDonough and S.-S. Sun. The composition of the earth. *Chemical geology*, 120(3-4):223–253, 1995.
- Y. Miyazaki and J. Korenaga. On the timescale of magma ocean solidification and its chemical consequences: 1. thermodynamic database for liquid at high pressures. *Journal of Geophysical Research: Solid Earth*, 124(4):3382–3398, 2019.
- W. B. Moore and A. A. G. Webb. Heat-pipe earth. *Nature*, 501(7468):501–505, 2013.
- J. P. Morgan and W. J. Morgan. Two-stage melting and the geochemical evolution of the mantle: a recipe for mantle plum-pudding. *Earth and Planetary Science Letters*, 170(3):215–239, 1999.
- F. D. Munch, A. Khan, B. Tauzin, M. van Driel, and D. Giardini. Seismological evidence for thermochemical heterogeneity in earth's continental mantle. *Earth and Planetary Science Letters*, 539:116240, 2020.
- M. Murakami. Chemical composition of the earth's lower mantle: Constraints from elasticity. *Physics and Chemistry of the Deep Earth, Part-2*, 2013. .
- M. Murakami, H. K., N. Sata, and Y. Ohishi. Post-perovskite phase transition and mineral chemistry in the pyrolitic lowermost mantle. *Geophys. Res. Lett.*, 32:L03304, 2005. .
- M. Murakami, S. V. Sinogeikin, H. Hellwig, J. D. Bass, and J. Li. Sound velocity of $mgsio_3$ perovskite to mbar pressure. *Earth Planet. Sci. Lett.*, 256:47–54, 2007a. .
- M. Murakami, S. V. Sinogeikin, J. D. Bass, N. Sata, Y. Ohishi, and K. Hirose. Sound velocity of $mgsio_3$ post-perovskite phase: A constraint on the d " discontinuity. *Earth Planet. Sci. Lett.*, 259:18–23, 2007b. .
- M. Murakami, Y. Asahara, Y. Ohishi, N. Hirao, and K. Hirose. Development of in situ brillouin spectroscopy at high pressure and high temperature with synchrotron radiation and infrared laser heating system: Application to the earth's deep interior. *Phys. Earth Planet. Inter.*, 174:282–291, 2009a. .
- M. Murakami, Y. Ohishi, N. Hirao, and K. Hirose. A perovskitic lower mantle inferred from high-pressure, high-temperature sound velocity data. *Nature*, 485:90–94, 2012. .
- R. Myhill, S. Cottaar, T. Heister, I. Rose, C. Unterborn, J. Dannberg, and R. Gassmoeller. Burnman – a python toolkit for planetary geophysics, geochemistry and thermodynamics. *Journal of Open Source Software*, 8(87):5389, 2023. .
- F. Nabiei, J. Badro, C.-É. Boukaré, C. Hébert, M. Cantoni, S. Borensztajn, N. Wehr, and P. Gillet. Investigating magma ocean solidification on earth through laser-heated diamond anvil cell experiments. *Geophysical Research Letters*, 48(12):e2021GL092446, 2021.
- T. Nakagawa and B. A. Buffett. Mass transport mechanism between the upper and lower mantle in numerical simulations of thermochemical mantle convection with multicomponent phase changes. *Earth and Planetary Science Letters*, 230(1-2):11–27, 2005.
- M. Nakajima and D. J. Stevenson. Melting and mixing states of the earth's mantle after the moon-forming impact. *Earth and Planetary Science Letters*, 427:286–295, 2015.
- E. Nisbet, M. Cheadle, N. Arndt, and M. Bickle. Constraining the potential temperature of the archaean mantle: a review of the evidence from komatiites. *Lithos*, 30(3-4):291–307, 1993.
- R. Nomura, K. Hirose, K. Uesugi, Y. Ohishi, A. Tsuchiyama, A. Miyake, and Y. Ueno. Low core-mantle boundary temperature inferred from the solidus of pyrolite. *Science*, 343(6170):522–525, 2014.

- C. O'Neill and S. Zhang. Lateral mixing processes in the hadean. *Journal of Geophysical Research: Solid Earth*, 123(8):7074–7089, 2018.
- H. S. C. O'Neill and H. Palme. *Composition of the silicate Earth: implications for accretion and core formation*, pages 3–126. Cambridge Univ. Press, 1998.
- H. S. C. O'Neill and H. Palme. Collisional erosion and the non-chondritic composition of the terrestrial planets. *Philosophical Transactions of the Royal Society A: Mathematical, Physical and Engineering Sciences*, 366(1883):4205–4238, 2008.
- H. S. C. O'Neill, D. Canil, and D. C. Rubie. Oxide-metal equilibria to 2500° c and 25 gpa: Implications for core formation and the light component in the earth's core. *Journal of Geophysical Research: Solid Earth*, 103(B6):12239–12260, 1998.
- H. Palme and H. S. C. O'Neill. *Cosmochemical estimates of mantle composition*, pages 1–39. Elsevier, 2014.
- A. S. Piazzoni, G. Steinle-Neumann, H.-P. Bunge, and D. Dolejš. A mineralogical model for density and elasticity of the earth's mantle. *Geochemistry, Geophysics, Geosystems*, 8(11), 2007. .
- H. Piet, J. Badro, F. Nabiei, T. Dennenwaldt, S.-H. Shim, M. Cantoni, C. Hébert, and P. Gillet. Spin and valence dependence of iron partitioning in earth's deep mantle. *Proceedings of the National Academy of Sciences*, 113(40):11127–11130, 2016.
- J.-P. Poirier. Light elements in the earth's outer core: a critical review. *Physics of the earth and planetary interiors*, 85(3-4):319–337, 1994.
- I. S. Puchtel, J. Blichert-Toft, M. F. Horan, M. Touboul, and R. J. Walker. The komatiite testimony to ancient mantle heterogeneity. *Chemical Geology*, 594:120776, 2022.
- Y. Ricard, E. Mattern, and J. Matas. Synthetic tomographic images of slabs from mineral physics. *Washington DC American Geophysical Union Geophysical Monograph Series*, 160:283–300, Jan. 2005. .
- A. Ricolleau, Y. Fei, A. Corgne, J. Siebert, and J. Badro. Oxygen and silicon contents of earth's core from high pressure metal–silicate partitioning experiments. *Earth and Planetary Science Letters*, 310(3-4):409–421, 2011.
- A. E. Ringwood. Chemical evolution of the terrestrial planets. *Geochimica et Cosmochimica Acta*, 30(1):41–104, 1966.
- A. E. Ringwood. Composition and petrology of the earth's mantle. *MacGraw-Hill*, 618, 1975.
- A. E. Ringwood. *Origin of the Earth and Moon*. Springer Science & Business Media, 1979.
- M. L. Rudolph, V. Lekić, and C. Lithgow-Bertelloni. Viscosity jump in earth's mid-mantle. *Science*, 350(6266):1349–1352, 2015.
- B. S. A. Schuberth, H. P. Bunge, and J. Ritsema. Tomographic filtering of high-resolution mantle circulation models: Can seismic heterogeneity be explained by temperature alone? *Geochemistry, Geophysics, Geosystems*, 10(5):Q05W03, May 2009. .
- G. E. Shephard, C. Houser, J. W. Hernlund, J. J. Valencia-Cardona, R. G. Trønnes, and R. M. Wentzcovitch. Seismological expression of the iron spin crossover in ferropericlae in the earth's lower mantle. *Nature Communications*, 12(1):5905, 2021.
- R. Sinmyo, H. K., D. Nishio-Hamane, Y. Seto, K. Fujino, N. Sata, and Y. Ohishi. Partitioning of iron between perovskite/postperovskite and ferropericlae in the lower mantle. *J. Geophys. Res.*, 113:204, 2008. .
- S. V. Sinogeikin and J. D. Bass. Single-crystal elasticity of pyrope and mgo to 20 gpa by brillouin scattering in the dia-mond cell. *Phys. Earth Planet. Inter.*, 120:43–62, 2000. .
- E. Sizova, T. Gerya, M. Brown, and L. Perchuk. Subduction styles in the precambrian: insight from numerical experiments. *Lithos*, 116(3-4):209–229, 2010.
- V. Solomatov. Magma oceans and primordial mantle differentiation, treatise on geophysics, vol. 9, 2015.
- P. A. Sossi, S. M. Eggins, R. W. Nesbitt, O. Nebel, J. M. Hergt, I. H. Campbell, H. S. C. O'Neill, M. Van Kranendonk, and D. R. Davies. Petrogenesis and geochemistry of archean komatiites. *Journal of Petrology*, 57(1):147–184, 2016.

- P. A. Sossi, O. Nebel, H. S. C. O'Neill, and F. Moynier. Zinc isotope composition of the earth and its behaviour during planetary accretion. *Chemical Geology*, 477:73–84, 2018.
- J. G. Spray. Upper mantle segregation processes: evidence from alpine-type peridotites. *Geological Society, London, Special Publications*, 42(1):29–40, 1989.
- L. Stixrude and C. Lithgow-Bertelloni. Thermodynamics of mantle minerals — I. Physical properties. *Geophysical Journal International*, 162(2):610–632, 08 2005a. ISSN 0956-540X. .
- L. Stixrude and C. Lithgow-Bertelloni. Thermodynamics of mantle minerals-i. physical properties. *Geophysical Journal International*, 162:610–632, 2005b. .
- L. Stixrude and C. Lithgow-Bertelloni. Thermodynamics of mantle minerals – ii. phase equilibria. *Geophysical Journal International*, 184(3):1180–1213, 2011a. .
- L. Stixrude and C. Lithgow-Bertelloni. Thermodynamics of mantle minerals-ii. phase equilibria. *Geophysical Journal International*, 184:1180–1213, 2011b. .
- L. Stixrude and C. Lithgow-Bertelloni. Thermal expansivity, heat capacity and bulk modulus of the mantle. *Geophysical Journal International*, 228(2):1119–1149, 09 2021. ISSN 0956-540X. .
- P. J. Tackley, S. Xie, T. Nakagawa, and J. W. Hernlund. Numerical and laboratory studies of mantle convection: Philosophy, accomplishments, and thermochemical structure and evolution. *GEOPHYSICAL MONOGRAPH-AMERICAN GEOPHYSICAL UNION*, 160(83):2190, 2005.
- B. Tauzin, L. Waszek, M. D. Ballmer, J. C. Afonso, and T. Bodin. Basaltic reservoirs in the earth's mantle transition zone. *Proceedings of the National Academy of Sciences*, 119(48):e2209399119, 2022. .
- I. Tolstikhin and A. W. Hofmann. Early crust on top of the earth's core. *Physics of the Earth and Planetary Interiors*, 148(2-4):109–130, 2005.
- J. Trampert, F. Deschamps, J. Resovsky, and D. Yuen. Probabilistic tomography maps chemical heterogeneities throughout the lower mantle. *Science*, 306(5697):853–856, 2004.
- N. Tsujino, D. Yamazaki, Y. Nishihara, T. Yoshino, Y. Higo, and Y. Tange. Viscosity of bridgmanite determined by in situ stress and strain measurements in uniaxial deformation experiments. *Science Advances*, 8(13):eabm1821, 2022.
- K. Umemoto and K. Hirose. Chemical compositions of the outer core examined by first principles calculations. *Earth and Planetary Science Letters*, 531:116009, 2020.
- D. G. Van Der Meer, W. Spakman, D. J. Van Hinsbergen, M. L. Amaru, and T. H. Torsvik. Towards absolute plate motions constrained by lower-mantle slab remnants. *Nature Geoscience*, 3(1):36–40, 2010.
- K. Vilella, T. Bodin, C.-E. Boukaré, F. Deschamps, J. Badro, M. D. Ballmer, and Y. Li. Constraints on the composition and temperature of llsvps from seismic properties of lower mantle minerals. *Earth and Planetary Science Letters*, 554:116685, 2021.
- M. Walter, E. Nakamura, R. Trønnes, and D. Frost. Experimental constraints on crystallization differentiation in a deep magma ocean. *Geochimica et Cosmochimica Acta*, 68(20):4267–4284, 2004.
- M. J. Walter. Melting of garnet peridotite and the origin of komatiite and depleted lithosphere. *Journal of petrology*, 39(1):29–60, 1998.
- M. J. Walter. Melt extraction and compositional variability in mantle lithosphere. *Treatise on geochemistry*, 2:568, 2003.
- J. T. Wasson and G. W. Kallemeyn. Compositions of chondrites. *Philosophical Transactions of the Royal Society of London. Series A, Mathematical and Physical Sciences*, 325(1587):535–544, 1988.
- L. Waszek, N. C. Schmerr, and M. D. Ballmer. Global observations of reflectors in the mid-mantle with implications for mantle structure and dynamics. *Nature communications*, 9(1):1–13, 2018.
- L. Waszek, B. Tauzin, N. C. Schmerr, M. D. Ballmer, and J. C. Afonso. A poorly mixed mantle transition zone and its thermal state inferred from seismic waves. *Nature Geoscience*, 14(12):949–955, 2021.
- D. J. Weidner. A mineral physics test of a pyrolite mantle. *Geophysical Research Letters*, 12(7):

- 417–420, 1985.
- D. J. Weidner, K. Swyler, and H. R. Carleton. Elasticity of microcrystals. *Geophysical Research Letters*, 2:189–192, 1975. .
- A. H. Wilson. The late-paleoarchean ultra-depleted comondale komatiites: Earth’s hottest lavas and consequences for eruption. *Journal of Petrology*, 60(8):1575–1620, 2019.
- G. Witt-Eickschen, H. Palme, H. S. C. O’neill, and C. M. Allen. The geochemistry of the volatile trace elements as, cd, ga, in and sn in the earth’s mantle: New evidence from in situ analyses of mantle xenoliths. *Geochimica et Cosmochimica Acta*, 73(6):1755–1778, 2009.
- R. K. Workman and S. R. Hart. Major and trace element composition of the depleted morb mantle (dmm). *Earth and Planetary Science Letters*, 231(1-2):53–72, 2005.
- L. Xie, A. Yoneda, D. Yamazaki, G. Manthilake, Y. Higo, Y. Tange, N. Guignot, A. King, M. Scheel, and D. Andrault. Formation of bridgmanite-enriched layer at the top lower-mantle during magma ocean solidification. *Nature communications*, 11(1):548, 2020.
- F. Xu, D. Yamazaki, N. Sakamoto, W. Sun, H. Fei, and H. Yurimoto. Silicon and oxygen self-diffusion in stishovite: Implications for stability of sio₂-rich seismic reflectors in the mid-mantle. *Earth and Planetary Science Letters*, 459:332–339, 2017.
- W. Xu, C. Lithgow-Bertelloni, L. Stixrude, and J. Ritsema. The effect of bulk composition and temperature on mantle seismic structure. *Earth and Planetary Science Letters*, 275(1-2):70–79, 2008.
- Y. Xu, T. J. Shankland, and B. T. Poe. Laboratory-based electrical conductivity in the earth’s mantle. *Journal of Geophysical Research: Solid Earth*, 105(B12):27865–27875, 2000.
- J. Yan, M. D. Ballmer, and P. J. Tackley. The evolution and distribution of recycled oceanic crust in the Earth’s mantle: Insight from geodynamic models. *Earth Planet. Sci. Lett.*, 537(116171), 2020. .
- R. Yang and Z. Wu. Elastic properties of stishovite and the cacl₂-type silica at the mantle temperature and pressure: An ab initio investigation. *Earth and Planetary Science Letters*, 404:14–21, 2014.
- S. Yoneda and L. Grossman. Condensation of caomg₂o₃sio₂ liquids from cosmic gases. *Geochimica et Cosmochimica Acta*, 59(16):3413–3444, 1995.
- T. Yoshizaki and W. F. McDonough. Earth and mars–distinct inner solar system products. *Geochemistry*, 81(2):125746, 2021.
- A. Zunino, J. A. D. Connolly, and A. Khan. Pre-Calculated Phase Equilibrium Models for Geophysical Properties of the Crust and Mantle as a Function of Composition. *Geochem. Geophys. Geosyst.*, 12(Q04001), 2011. .

Table 1 Summary of geophysical estimates of lower mantle composition and thermal state. Only mean values are indicated, but uncertainties on temperature and Mg/Si, where no ranges are given, are at least $\pm 10\%$. For more details the reader is referred to the original studies. [A] Radial seismic reference model; [B] ISC global mantle P- and S-wave travel times, fundamental spheroidal and toroidal normal modes, and mass; [C] Global electromagnetic induction data and mean mass and moment of inertia; [D] ISC global mantle P- and S-wave travel times and mean mass and moment of inertia; [E] Normal modes, mantle and core body wave travel times, mean mass and moment of inertia, and tidal response.

Study	Temperature at top of LM	Temperature at CMB	LM thermal gradient	LM Mg/Si (mol)	Observational constraints	Comparison
Jackson (1998)	1850 K	2300 K	adiabatic	1.27	A	forward model
Marton & Cohen (2002)	1800 K	2400 K	adiabatic	1.27	A	forward model (ab initio)
da Silva et al. (2000)	1900 K	4000 K	superad.	1.27	A	forward model (ab initio)
Deschamps & Trampert (2004)	–	3750 K	superad.	1.27	A	random sampling
Cammarano et al. (2005)	1873 K	2400 K	adiabatic	1.27	B	random sampling
Matterm et al. (2005)	1800 K 2200 K 2500 K	2000 K 2500 K 2700 K	subad. subad. subad.	1.27 1.07 1.03	A	Inversion
Khan et al. (2006)	1900 K	3200 K	superad.	1.09	C	Inversion
Matas et al. (2007)	1935 K 1926 K 1875 K	Temperature at 810 km depth. Temperature at 810 km depth. Temperature at 810 km depth.	superad. superad. superad.	1.03 1.07 1.27	A	Inversion
Khan et al. (2008)	1700 K	2700 K	superad.	1.35	D	inversion
Cobden et al. (2009)	1900 K	3100 K Temperature at 2500 km depth.	superad.	1.0–1.4 ^c	A	Inversion
Kemper et al. (2023)	1900 K	2600 K	isentropes	≥ 1.4	E	Inversion

Table 2 Thermoelastic properties of lower mantle phases. V_0 : ambient volume; G_0 & G' : shear modulus at ambient pressure and temperature and its pressure derivative; K_{T0} & K'_T : isothermal bulk modulus at ambient pressure and temperature and its pressure derivative; K_{S0} & K'_S : adiabatic bulk modulus at ambient pressure and temperature and its pressure derivative; θ_0 : Debye temperature; γ_0 : Grüneisen parameter; η_{S0} : shear strain derivative of γ_0 ; $q = \frac{\partial \ln \eta}{\partial \ln V}$.

Formula Phase	Reference	P (GPa)	V_0 (cm ³ /mol)	G_0 (GPa)	G'	K_{T0} (GPa)	K'_T	K_{S0} (GPa)	K'_S	θ_0 (K)	γ_0	η_{S0}	q
<u>Polycrystalline study</u>													
MgO, periclase	Murakami et al., [2009b]	14-129	11.24	125.2	2.14	152 ^b	4 ^b	163 ^a	3.8 ^a				
Mg _{0.92} Fe _{0.08} O HS, ferropericlase	Murakami et al., [2012]	0-120	11.32	112.2	2.07	170 ^b	4 ^b						
Mg _{0.92} Fe _{0.08} O LS, ferropericlase	Murakami et al., [2012]	0-120	11.03	127.9	1.99	170 ^b	4 ^b						
MgSiO ₃ : bridgmanite	Murakami et al., [2007a]	8-96	24.43	169.6	1.73			257.1 ^c	3.71 ^c				
MgSiO ₃ + 4 wt% Al ₂ O ₃ , bridgmanite	Murakami et al., [2012]	42-124	24.51	162.2	1.81			252 ^d	3.7 ^d				
Mg _{0.93} Fe _{0.07} Fe _{0.02} Si _{0.98} O ₃ , bridgmanite	Mashino et al., [2020]	26-105	24.54	168.4	1.73	256 ^e	4 ^e						
Mg _{0.86} Fe _{0.15} Fe _{0.03} Si _{0.97} O ₃ , bridgmanite	Mashino et al., [2020]	26-124	24.64	167	1.74	257 ^f	4 ^f						
<u>Single-crystal study</u>													
Mg _{0.9} Fe _{0.1} O, ferropericlase	Marguardt et al., [2009]	0-70	11.34	120	2.05	151	4.1						
MgSiO ₃ : bridgmanite	Criniti et al., [2021]	0-79		175.6	1.86			257.1	3.71				
Mg _{0.88} Fe _{0.1} Al _{0.14} Si _{0.9} O ₃ , bridgmanite	Fu et al., [2023]	25-82		211*	1.66*			326*	3.32*				
<u>Two-phase aggregate modelling</u>													
Mg _{0.79} Fe _{0.21} O HS, ferropericlase	This study		11.45 ^g	104	1.88	158 ^b	4 ^b			686 ^g	1.39 ^g	2.2 ^g	1.7 ^g
Mg _{0.79} Fe _{0.21} O LS, ferropericlase	This study		11.17 ^g	113	1.84	170 ^b	4 ^b			686 ^g	1.39 ^g	2.2 ^g	1.7 ^g
X _{Fe} = 0.06 + 4 wt% Al ₂ O ₃ , bridgmanite	This study		24.50	164.4	1.77			251 ⁱ	3.86 ⁱ	905 ^h	1.57 ^h	2.6 ^h	1.1 ^h
X _{Fe} = 0.1 + 4 wt% Al ₂ O ₃ , bridgmanite	This study		24.57	163.3	1.76			249 ⁱ	3.90 ⁱ	905 ^h	1.57 ^h	2.6 ^h	1.1 ^h

* values at 25 GPa.

^a Sinogeikin and Bass (2000)

^b Fei et al. (2007)

^c Criniti et al. (2021)

^d Jackson et al. (2005)

^e Dorflman and Duffy (2014)

^f Lundin et al. (2008)

^g Myhill et al. (2023)

^h Stixrude and Lithgow-Bertelloni (2011b)

ⁱ Fu et al. (2023)